

Measuring the quartic Higgs self-coupling at a multi-TeV muon collider

Mauro Chiesa^a, Fabio Maltoni^{b,c}, Luca Mantani^{b,d}, Barbara Mele^e,
Fulvio Piccinini^f, Xiaoran Zhao^b

(a) CNRS, LAPTh, 9 Chemin de Bellevue, 74940 Annecy, France

(b) Centre for Cosmology, Particle Physics and Phenomenology (CP3),

Université Catholique de Louvain, Chemin du Cyclotron, B-1348 Louvain la Neuve, Belgium

(c) Dipartimento di Fisica e Astronomia, Università di Bologna e INFN, Sezione di Bologna,
via Irnerio 46, I-40126 Bologna, Italy

(d) Institut für Theoretische Physik, Universität Heidelberg, Germany

(e) INFN, Sezione di Roma, c/o Dipartimento di Fisica, "Sapienza" Università di Roma, P.le
Aldo Moro 2, I-00185 Rome, Italy

(f) INFN, Sezione di Pavia, Via A. Bassi 6, I-27100 Pavia, Italy

ABSTRACT

Measuring the shape of the Higgs boson potential is of paramount importance, and will be a challenging task at current as well as future colliders. While the expectations for the measurement of the trilinear Higgs self-coupling are rather promising, an accurate measurement of the quartic self-coupling interaction is presently considered extremely challenging even at a future 100 TeV proton-proton collider. In this work we explore the sensitivity that a muon collider with a center of mass energy in the multi-TeV range and luminosities of the order of $10^{35} \text{cm}^{-2} \text{s}^{-1}$, as presently under discussion, might provide, thanks to a rather large three Higgs-boson production and to a limited background. By performing a first and simple analysis, we find a clear indication that a muon collider could provide a determination of the quartic Higgs self-coupling that is significantly better than what is currently considered attainable at other future colliders.

1 Introduction

The Higgs boson discovery at the LHC in 2012 [1, 2] and the subsequent campaign of measurements of its properties [3, 4], have provided a wonderful confirmation of our understanding of elementary particles and their interactions at the weak scale. So far, the predictions of the Standard Model (SM) for the Higgs boson couplings to the vector bosons and to third generation fermions are in spectacular agreement with observations [5, 6, 7, 8]. On the other hand, its interactions with lighter sectors, such as the first and second generation quarks and leptons, are still to be confirmed. In addition, the very existence of a scalar doublet has opened many possibilities for new physics to couple to the SM as well as many new avenues for searching for it. Leading, yet simple examples are Higgs portals to singlet fermions and/or scalars, which could provide a solution to open questions such as that of the nature of dark matter or the origin of matter-anti-matter asymmetry in the universe. Other possibilities could involve extended charged scalar sectors, which in turn could point to the existence of new symmetries, such as supersymmetry. All such possibilities are continuously pushed at higher scales by the accuracy of the measurements of the Higgs-boson couplings to the heavier SM particles, which is presently $\mathcal{O}(10\%)$ [3, 4]. The high luminosity phase (HL-LHC) will improve the corresponding accuracy to a few percents for the vector bosons and third generation, and access for the first time the couplings to the second generation fermions [9, 10].

One key sector, which is currently very weakly constrained and could very easily hide or be connected to new physics, is the scalar potential [10, 11]. In the SM, the Higgs scalar potential is fixed by just two low energy parameters, the Higgs mass ($m_H \simeq 125$ GeV) and the Fermi constant G_F (or equivalently the vacuum expectation value $v \simeq 246$ GeV). At the weak scale, the potential can be written in terms of the Higgs trilinear (λ_3) and quartic (λ_4) self-couplings

$$V(H) = \frac{1}{2}m_H^2 H^2 + \lambda_3 v H^3 + \frac{1}{4}\lambda_4 H^4, \quad (1)$$

where in the SM, $\lambda_3 = \lambda_4 = m_H^2/2v^2 \equiv \lambda_{SM}$. In particular, higher-point Higgs boson self interactions are forbidden by the request of renormalisability of the SM up to arbitrarily high scales.

The measurement of the parameters that describe the shape of the Higgs potential are therefore a milestone in the quest of understanding the mechanism of the electroweak symmetry breaking and of exploration of new physics. The relevance of this information on the one hand, and the inherent experimental challenges on the other hand, make this measurement one of the most relevant benchmarks that can be employed to set the physics potential of future high-energy collider projects.

The determination of the trilinear Higgs self-couplings λ_3 at the LHC and at future colliders has been vastly considered in the literature, from measurements involving Higgs boson pair production and through radiative effects in single Higgs production (see for instance [10] and [12]). At the end of the complete FCC programme [13, 14, 15] one expects to reach a $\mathcal{O}(5\%)$ accuracy on λ_3 [13].

Although in SM extensions where new physics is at higher scales, λ_4 is related to λ_3 , an unbiased determination of the Higgs quartic self-coupling will require a measurement of processes

genuinely depending on λ_4 , like the triple Higgs production.¹

The measurement of the triple Higgs production cross section, currently being the most studied handle on the quartic Higgs self-coupling, looks very challenging even at the 100 TeV proton collisions foreseen at the FCC-hh. Quite a number of studies concerning different final states deriving from various combinations of the Higgs decay channels have been considered, see [12]. The expected constraint on a λ_4 deviation (for a SM value of λ_3) is quite poor [19, 20, 21], the most optimistic estimate obtained from HHH production with $6b$ in the final state is $\lambda_4/\lambda_4^{\text{SM}} \in [-2, +13]$ (at 2σ , with $\lambda_3 = \lambda_3^{\text{SM}}$) with a significance for SM HHH production of about 2σ with 20 ab^{-1} of integrated luminosity (and perfect b -tagging) [22]. Indirect bounds on the quartic Higgs self-coupling can be obtained from one-loop contributions in HH final states at future lepton and hadron colliders (see Refs. [12, 16, 17, 18] and references therein) and these contributions allow to constrain $\lambda_4/\lambda_4^{\text{SM}}$ at FCC-hh in the range $[-2.3, +4.3]$ at 1σ for $\lambda_3 = \lambda_3^{\text{SM}}$ [12].

The aim of the present study is to explore for the first time the reach of a multi-TeV muon collider for a complete reconstruction of the shape of the Higgs potential. In connection with the discussion on next generation high-energy colliders carried out for the 2020 European Strategy Update on Particle Physics [23], a very attractive option was given by the possibility of a high-luminosity multi-TeV muon collider [24]. In particular, a collider with center of mass (c.m.) energies in the range 1.5 to 14 TeV, and luminosities up to $\mathcal{O}(10^{35}) \text{ cm}^{-2}\text{s}^{-1}$ is presently under consideration. Although a long and challenging period of further accelerator research and development is still needed to prove the actual feasibility of such a machine, its physics opportunities seem extremely wide and rich and therefore need to be carefully assessed.

There are a number of immediate and crucial advantages in replacing electrons with muons in lepton collisions, that would allow to amazingly extend the effective collision energy in realistic colliders. For instance, in the LHC tunnel, one might implement 14 TeV muon collisions [25], whose discovery potential in direct searches of heavy (SM charged) states would be roughly similar to the one of a 100 TeV proton collider of similar luminosity [24]. In addition, accelerating muons could offer a very cost-effective way to increase the lepton collision energy reach, while keeping the beam energy spread one order of magnitude smaller than for an electron collider of similar c.m. energy [26]. Finally, progress on long-standing hurdles has been recently achieved. For example, preliminary studies show that potentially serious beam-induced background effects arising from the beam muon decays could be manageable as they become less severe at higher c.m. energies [27, 28]. Nevertheless, collecting data in the forward regions in such a high-background environment might be challenging, and need more ideas and developments [37, 38, 39, 40, 41].

In the following, we assume four hypothetical setups for the c.m. energy and luminosity as references: $\sqrt{s} \simeq [1.5, 3, 6, 14] \text{ TeV}$ and $\mathcal{L} \simeq [1.2, 4.4, 12, 33] \cdot 10^{34} \text{ cm}^{-2}\text{s}^{-1}$, respectively. These configurations are based on the parameters characterizing present muon collider designs according to the MAP scheme [26, 29, 30, 25].² In addition, we will consider two further collision energies/luminosities, i.e. $\sqrt{s} \simeq [10, 30] \text{ TeV}$ and $\mathcal{L} \simeq [20, 100] \cdot 10^{34} \text{ cm}^{-2}\text{s}^{-1}$, respectively, motivated by the required scaling of the luminosity needed to compensate the $1/s$ decrease in the s -channel cross sections that are relevant for pair production of new heavy objects [24].

¹Double Higgs production is sensitive to λ_4 through loop effects, see [16, 17, 18].

²For machine designs using resonant production of muon pairs at threshold from e^+e^- collisions, see [31, 32].

\sqrt{s} (TeV)	1.5	3	6	10	14	30
\mathcal{L} ($10^{34} \text{ cm}^{-2} \text{ s}^{-1}$)	1.2	4.4	12	20	33	100
L_{10y} (ab^{-1})	1.2	4.4	12	20	33	100

Table 1: Reference muon collision energies \sqrt{s} , and instantaneous luminosities \mathcal{L} , with corresponding integrated luminosities L for a 10 years run (one year of $\sim 10^7$ s). The luminosity values assumed for $\sqrt{s} \simeq (1.5, 3, 6, 14)$ TeV are as from [26, 30].

The setups are summarized in table 1, where for each \sqrt{s} value we also report the integrated luminosity (L) collected over a ten-year run (with a conventional year of 10^7 seconds).

A high-luminosity multi-TeV muon collider has a physics potential both for direct searches of heavy objects as well as for precision measurements [24]. As a prime example of the latter, in this work, we focus on its capability to constrain the SM Higgs scalar potential. The reach of such a measurement builds up on the clean environment of lepton collisions, where QCD backgrounds are moderate, which also allows events to be recorded in absence of a trigger. A few percent determination of the trilinear Higgs self-coupling λ_3 via double Higgs production, eventually even better than that achievable at the FCC, seems possible at the moment [24], although only simplified studies are available [33].

In this paper, we provide a first quantitative analysis of the muon collider potential to access information on the *quartic* Higgs self-coupling λ_4 as obtained from direct measurements of the cross section for triple Higgs-boson production. We will consider in particular the multi-TeV energy and order $10^{35} \text{ cm}^{-2} \text{ s}^{-1}$ luminosity options considered in table 1. Since, for $\sqrt{s} \gtrsim 1.5$ TeV, vector-boson-fusion channels (whose cross sections grow as $\log s$) get the upper-hand on the corresponding s -channel production mediated by the $\mu^+ \mu^- \rightarrow HHHZ^*$ process, our analysis will be mainly focused on the W-boson-fusion (WBF) process

$$\mu^+ \mu^- \rightarrow W^* W^* \nu_\mu \bar{\nu}_\mu \rightarrow HHH \nu_\mu \bar{\nu}_\mu. \quad (2)$$

Depending on the particular Higgs decay channel involved, the final signature of triple Higgs events can be quite diverse [19], although a few kinematical common features (like the presence of three systems resonating at the Higgs masses) will be universal. Thanks to these features, even dijet final states, such as the b -jets from high-rate $H \rightarrow b\bar{b}$ decays, are expected to be efficiently reconstructed.³

In this study, we work under two main hypotheses. First, we assume that a number of potential machine and detector issues will be solved after detailed studies, possibly involving innovative technologies, and discuss the potential consequences of just having at disposal signal event statistics for triple Higgs bosons corresponding to such high c.m. energies and luminosities as envisaged in the MAP project. Second, we assume that the bulk of the different HHH final states corresponding to the dominant Higgs decay channels can be reconstructed with high

³In fact, the final detection efficiency could be strongly affected by the machine-induced background and the machine detector interface that could seriously impact the final detector acceptance [27, 28]. In any case, it is clear that further research and development of accelerator, detector, and analysis technologies for a multi-TeV muon collider will be needed to reach robust conclusions on the physics potential of such a machine.

efficiency. Correspondingly, we estimate the muon collider sensitivity to detect a deviation in the Higgs λ_3 and λ_4 self-couplings through the full statistics of the triple Higgs production. On the other hand, as far as the Higgs trilinear self-coupling λ_3 is concerned, we do not consider here the stronger direct constraints that presumably can be obtained through the scrutiny of the higher-rate double Higgs production.

The plan of the paper is as follows. In Section 2 we present the results of our Monte Carlo simulations for the signal cross sections and distributions in the standard model, including a study of the acceptance of 6 b-jet final state.

In Section 3, we parametrise the cross sections dependence in new physics scenarios as a quartic polynomial of the deviations δ_3 and δ_4 of the self-couplings with respect to the SM predictions and study the sensitivity of representative distributions to them. Finally, we determine the constraining potential (considering different energy and luminosity setups) of a future muon collider. In the last section, we present our conclusions and the outlook.

2 Triple Higgs production in the standard model

In this section, we present the cross sections and a few kinematical distributions for the process

$$\mu^+\mu^- \rightarrow HHH \nu\bar{\nu}, \quad (3)$$

in the SM and in scenarios where the Higgs self-couplings are modified, at muon collider energies in the range [1.5, 30] TeV.

In figure 1, we show a few representative Feynman diagrams of the process. By inspection, one can quickly conclude that at the tree level, each diagram can be at most linearly dependent on the quartic self-coupling λ_4 , and linearly or quadratically dependent on λ_3 . In fact, the majority of diagrams are independent from Higgs self-couplings. This observation leads to the expectation that on the one hand, the cross section sensitivity to self-couplings in general and to the quartic coupling in particular, will be quite mild and on the other hand, a very precise knowledge of the WWH and $WWHH$ couplings will be needed in order to pin down the Higgs potential.

Triple Higgs production proceeds through two main classes of diagrams: the WBF channel ⁴

$$\mu^+\mu^- \rightarrow W^*W^*\nu_\mu\bar{\nu}_\mu \rightarrow HHH \nu_\mu\bar{\nu}_\mu, \quad (4)$$

and the s -channel

$$\mu^+\mu^- \rightarrow HHH Z^* \rightarrow HHH \nu_{e,\mu,\tau}\bar{\nu}_{e,\mu,\tau}. \quad (5)$$

Both sets contribute at the amplitude level to $\mu^+\mu^- \rightarrow HHH\nu\bar{\nu}$ yet, as we will discuss in the following, mostly in different phase space regions.

In order to compute the $\mu^+\mu^- \rightarrow HHH\nu\bar{\nu}$ cross sections and distributions, including the complete self-coupling dependence, we have used two Monte Carlo event generators: WHIZARD [34, 35] (version 2.6.4) and MADGRAPH5_AMC@NLO [36]. Even though the SM implementation in both codes does not allow the user to change λ_3 and λ_4 from the input cards, it is

⁴The corresponding cross sections for Z boson fusion, $\mu^+\mu^- \rightarrow Z^*Z^*\mu^+\mu^- \rightarrow HHH \mu^+\mu^-$ amount to 15–20% of the ones for W boson fusion, and are therefore relevant. We leave their inclusion to future work.

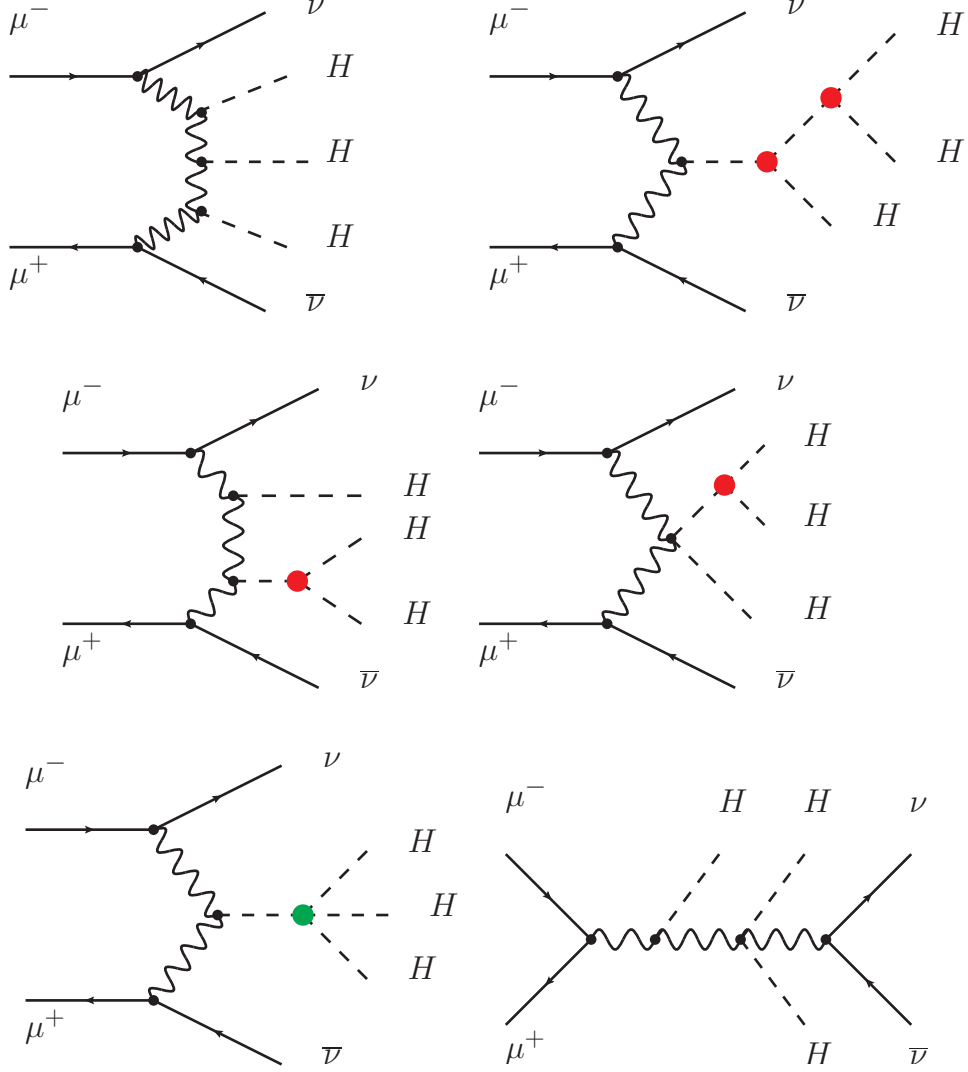


Figure 1: Representative Feynman diagrams contributing to the process $\mu^+\mu^- \rightarrow HHH\nu\bar{\nu}$ that do not involve self-couplings (top-left and bottom-right), involve the trilinear twice (top-right) and once (central), and the quartic (bottom-left) couplings. s -channel diagrams (bottom-right) contribute but become negligible at high energy (note that in this case $\nu = \nu_e, \nu_\mu, \nu_\tau$).

sufficiently easy to do that directly accessing the source codes.⁵ The Higgs and gauge boson widths as well as the muon mass (and Yukawa) are set to zero, in order to avoid issues with gauge cancellations at very high energy.

For all the results discussed in the following, we impose a technical generation cut $M_{\nu\bar{\nu}} > 150$ GeV on the neutrino pair invariant mass $M_{\nu\bar{\nu}}$, to prevent the singularity arising from a vanishing Z -boson width in the s -channel. The latter cut effectively takes away most of the s -channel contribution. The s -channel effects tend anyhow to be strongly suppressed at multi-TeV collision energies. After removing the Z -resonance contributions by the $M_{\nu\bar{\nu}} > 150$ GeV cut, we find that the relative off-shell contribution of the $\mu^+\mu^- \rightarrow HHH Z^* \rightarrow HHH \nu\bar{\nu}$ to the total cross section is about 2.5% at $\sqrt{s} \simeq 1.5$ TeV, $1.4 \cdot 10^{-3}$ at 3 TeV, and 10^{-4} at 6 TeV. With the present LO accuracy, our complete results for $\mu^+\mu^- \rightarrow HHH \nu\bar{\nu}$ will then match the ones for the WBF process $\mu^+\mu^- \rightarrow W^* W^* \nu_\mu \bar{\nu}_\mu \rightarrow HHH \nu_\mu \bar{\nu}_\mu$ with excellent accuracy in the energy range considered.⁶

In figure 2, we plot the $\mu^+\mu^- \rightarrow HHH \nu\bar{\nu}$ cross section versus \sqrt{s} in the SM. On the right axis we include the expected number of triple Higgs final states produced for an integrated luminosity $L=100$ ab $^{-1}$. The left-hand plot corresponds to the cross-sections results in a linear scale for two anomalous scenarios as obtained in WHIZARD, while on the right-hand side the MADGRAPH5_AMC@NLO results for the yield are plotted in a log-scale, also for two additional scenarios. We have carefully verified that the results from the two MC's agree within uncertainties for SM as well as in presence of anomalous interactions. We define $\delta_{3,4}$ and $\kappa_{3,4}$, through the following relations

$$\lambda_3 = \lambda_{SM}(1 + \delta_3) = \kappa_3 \lambda_{SM}, \quad (6)$$

$$\lambda_4 = \lambda_{SM}(1 + \delta_4) = \kappa_4 \lambda_{SM}, \quad (7)$$

which imply that the SM values for the couplings are recovered for $\delta_{3,4} = 0$, or equivalently for $\kappa_{3,4} = 1$. We point out that, for the sake of both simplicity and generality, we phrase our results in terms of the anomalous couplings above. At the perturbative level of our predictions, i.e., at the tree level, one can easily link the deformations of the λ 's to the coefficients of higher dimensional operators, see for instance [18]. The simplest instance is that of adding just one operator of dimension six, $c_6(\Phi^\dagger\Phi)^3/\Lambda^2$. In this case, one finds that the shifts in the trilinear and quartic couplings are related, i.e.,

$$\delta_4 = 6 \delta_3, \quad (\text{SMEFT at dim} = 6). \quad (8)$$

This constraint can be lifted by further adding operators of higher dimension, i.e., $c_8(\Phi^\dagger\Phi)^4/\Lambda^4$. As special case of the latter situation, one can fix the couplings of the six and eight dimensional operators, to only have the quartic coupling modified, $\delta_3 = 0$ and $\delta_4 \neq 0$. However, it is important to remind that this is not what is generically expected from the SMEFT and it implies a fine tuning, which is valid only at a given scale.

⁵In MADGRAPH5_AMC@NLO is also possible to use the SMEFT@NLO model.

⁶Note that interference effects between the WBF and s -channel diagrams are negligible due to the non-overlapping typical kinematics of the two configurations. For the reasons above, in MADGRAPH5_AMC@NLO we find it easier to directly exclude the s -channel contributions by actually simulating $e^+\mu^- \rightarrow HHH \nu_\mu \bar{\nu}_e$. We have explicitly checked that this approximation is excellent and make the simulations faster.

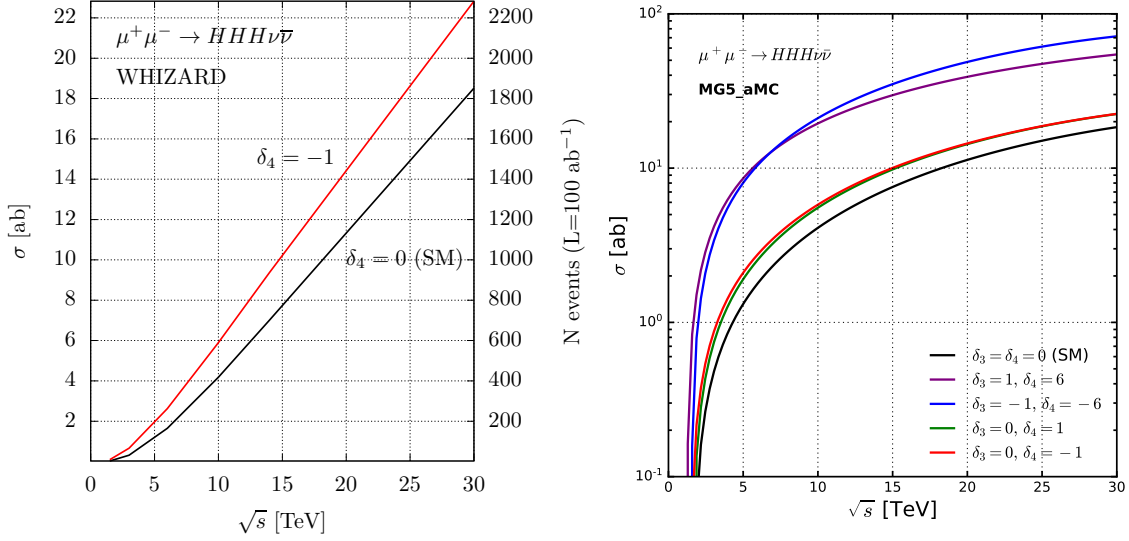


Figure 2: Expected cross sections (left) and signal event numbers for a reference integrated luminosity of 100 ab^{-1} (right) for $\mu^+\mu^- \rightarrow HHH\nu\bar{\nu}$ versus the c.m. collision energy, for $M_{\nu\nu} \gtrsim 150 \text{ GeV}$. Cross sections for different assumptions of the trilinear and quartic couplings are presented, as well as for the SM case, obtained by WHIZARD (left-hand side) and MADGRAPH5_AMC@NLO (right-hand side). Details on the scenarios are given in the text.

In order to get a first feeling of the cross section sensitivity to variations of the Higgs quartic coupling, in figures 2 we also show the cross section obtained by keeping the SM value for λ_3 and switching off λ_4 ($\delta_3 = 0, \delta_4 = -1$ or $\kappa_3 = 1, \kappa_4 = 0$). The effect is an increase, as expected from general arguments on unitarity cancellation, of production rates of about 20%–30% in the \sqrt{s} range considered here. On the right-hand plot, we show the corresponding results as obtained from MG5AMC also including two scenarios of interest: the $\delta_3 = \pm 1, \delta_4 = \pm 6$ cases, corresponding to relative shift between δ_3 and δ_4 consistent with an EFT approach, and a scenario $\delta_3 = 0, \delta_4 = +1$ with no change in λ_3 , yet a 100% increase of λ_4 . It is interesting to note that, as far as total rates are concerned, the latter case turns out to be hardly distinguishable from the scenario where $\lambda_3 = \lambda_{SM}$ and $\lambda_4 = 0$.

A second set of relevant information is provided in table 2, where we report the $\mu^+\mu^- \rightarrow HHH\nu\bar{\nu}$ total cross sections and event numbers⁷ for the reference set of collision energies and integrated luminosities of table 1. In addition to total cross sections, also the number of events close to threshold, i.e., with a requirement on the HHH -invariant-mass (M_{HHH}) to be less than 1 and 3 TeV is given. As we will discuss in the following, the sensitivity to the quartic coupling depends rather strongly on the phase space region occupied by the Higgs bosons in the final state, being the strongest close to threshold.

Given the very small cross section at 1.5 TeV (cf. table 2), we will not consider this option in our sensitivity studies. On the other hand, in section 4 we will include the case $\sqrt{s} = 3 \text{ TeV}$ even

⁷A cut $M_{\nu\nu} \gtrsim 150 \text{ GeV}$ will be implicit from now on.

\sqrt{s} (TeV) / L (ab ⁻¹)	1.5 / 1.2	3 / 4.4	6 / 12	10 / 20	14 / 33	30 / 100
σ_{SM} (ab) [N _{ev}]						
σ^{tot}	0.03 [0]	0.31 [1]	1.65 [20]	4.18 [84]	7.02 [232]	18.51 [1851]
$\sigma(M_{HHH} < 3 \text{ TeV})$	0.03 [0]	0.31 [1]	1.47 [18]	2.89 [58]	3.98 [131]	6.69 [669]
$\sigma(M_{HHH} < 1 \text{ TeV})$	0.02 [0]	0.12 [1]	0.26 [3]	0.37 [7]	0.45 [15]	0.64 [64]

Table 2: Cross sections and (in squared brackets) event numbers for triple Higgs production via the process $\mu^+\mu^- \rightarrow HHH\nu\bar{\nu}$, at collision energies and integrated luminosities as from table 1. A cut $M_{\bar{\nu}\nu} \gtrsim 150\text{GeV}$ is applied. The effect of imposing an upper cut on the HHH invariant mass is also detailed. Cross sections and corresponding event numbers refer to the SM case.

if the corresponding nominal luminosity is still too low to have a reasonable event statistics. Indeed, we will show how a (presently unrealistic) increase of a factor about 20 in luminosity (giving an integrated luminosity of 100 ab⁻¹) might make even a $\sqrt{s}=3$ TeV muon collider (or, equivalently, a CLIC collider at 3 TeV of comparable luminosity) sensitive to a δ_4 variation.

In figures 3, 4, 5 we plot the inclusive Higgs transverse momentum, the Higgs rapidity and the Higgs-pair ΔR distributions, with and without an upper cut of 1 TeV on the HHH invariant mass, respectively. We note that peak value of the transverse momentum is around 100 GeV, a value that turns out to be rather independent on the collider energy. The invariant mass cut at 1 TeV has a mild effect and only on the shapes of the distributions at higher energy collisions. On the other hand, the rapidity distributions are found to have a rather strong dependence on the collision energy and also on being at threshold. At high collision energy, the rapidity range become quite large reaching more than five units in rapidity. To be efficiently detected, such Higgs bosons would need a quite wide rapidity coverage of the detector. Finally, figure 5 shows that the most probable distance between two Higgs bosons is around π , extending to larger values at high energy, due to forward-backward Higgs production. At threshold, there is a very mild dependence on the collision energy.

In order to have a more complete understanding of the dynamics of a HHH event, in figure 6 we present the rapidity and ΔR distributions of each of the Higgs bosons ordered in p_T . The solid curves represent the inclusive sample with no lower or upper cut of 1 TeV on the M_{HHH} . By inspecting the two plots one concludes that at threshold the ordering of the Higgs in p_T has mild effect as the Higgs have comparable momenta. On the other hand, in far from threshold configurations, which dominate inclusive cross sections, two Higgs bosons are typically rather central and back-to-back, while the softest one is forward.

The plots in figure 4, obtained without imposing any acceptance cut to the final state (apart from identifying the threshold region by the cut $M_{HHH} < 1 \text{ TeV}$) show that at high energy the Higgs bosons tend to be produced in the forward region. At a muon collider, however, it is necessary to shield the detectors in the forward regions, in order to suppress the beam-induced background. As already mentioned in the introduction, this issue was addressed for the 1.5 TeV setup, see [37, 38, 39, 40, 41], where it was proposed to put nozzles with an angular opening between 5 and 10 degrees at the points where the beam enters the detector. Since at higher c.m. energies the beam induced radiation is expected to be more forward, the effective angular

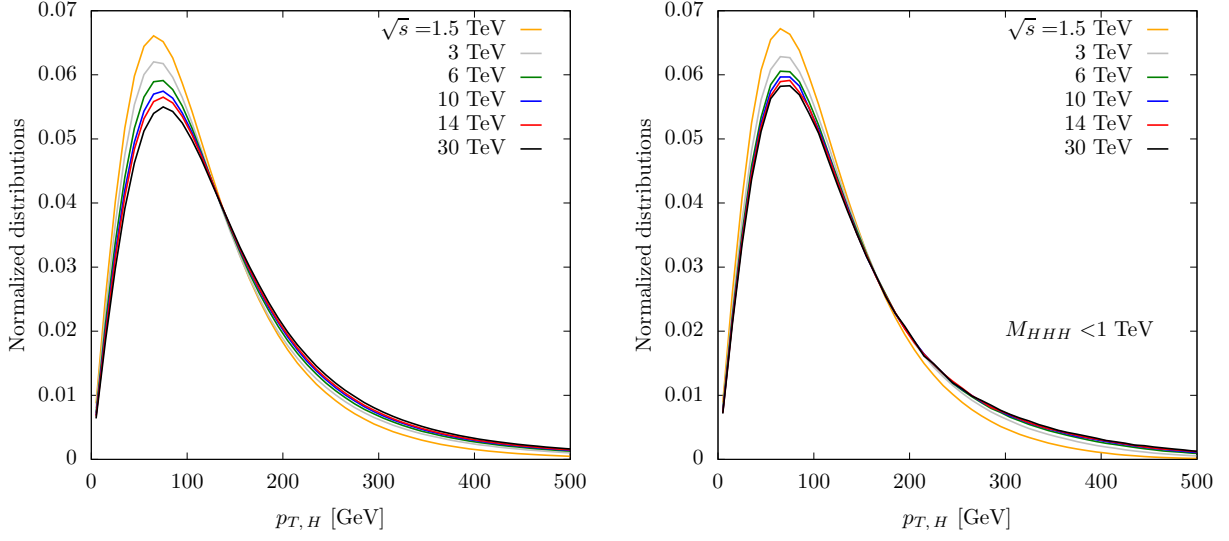


Figure 3: Inclusive Higgs transverse momentum distributions (normalized) for the $\mu^+\mu^- \rightarrow HHH\nu\bar{\nu}$ process, in the SM, at different collision energies. A technical cut of $M_{\nu\bar{\nu}} \gtrsim 150$ GeV is included. The plot on the right includes an upper cut of 1 TeV on the HHH invariant mass.

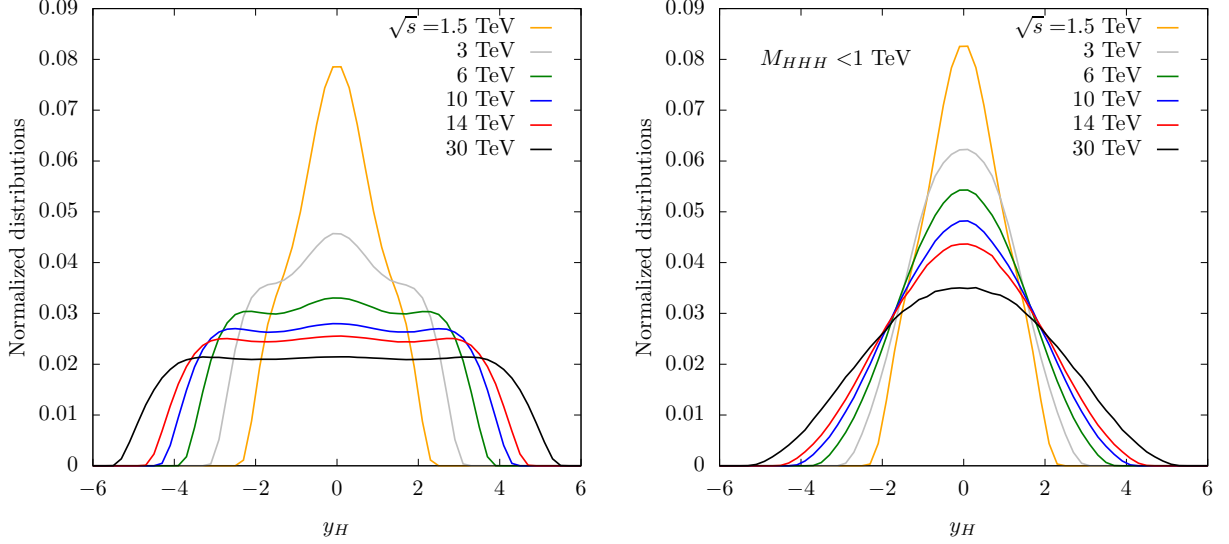


Figure 4: Inclusive Higgs rapidity distributions (normalized) for the $\mu^+\mu^- \rightarrow HHH\nu\bar{\nu}$ process, in the SM, at different collision energies. A technical cut of $M_{\nu\bar{\nu}} \gtrsim 150$ GeV is included. The plot on the right includes an upper cut of 1 TeV on the HHH invariant mass.

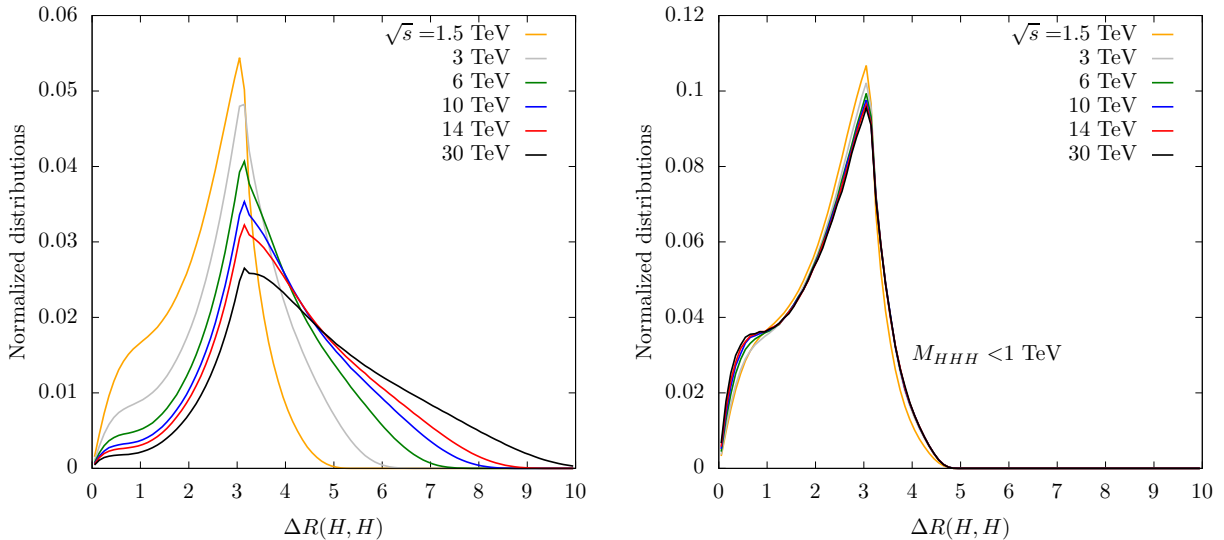


Figure 5: Inclusive ΔR distributions (normalized) for the $\mu^+\mu^- \rightarrow HHH\nu\bar{\nu}$ process, in the SM, at different collision energies. A technical cut of $M_{\nu\bar{\nu}} \gtrsim 150$ GeV is included. The plot on the right includes an upper cut of 1 TeV on the HHH invariant mass.

opening of the noozles might be decreased for the largest \sqrt{s} we are considering.

In order to study the impact of these limitations on the measurement of triple-Higgs production at the muon collider, in table 3 we collect the geometric acceptances corresponding to the energy setups in table 1, for different cuts on the transverse momentum and on the rapidity of the Higgs decay products. We consider two-body Higgs decays, which give the dominant contribution to the Higgs decay width. In particular, in our simulation the three Higgs bosons are still produced on-shell, and then decayed afterwards to $b\bar{b}$ pairs, with the acceptance cuts applied to the six final-state b quarks. The scaling of the acceptances as a function of the transverse-momentum and rapidity cuts can be read from table 3. Concerning the dependence on the rapidity cuts, this is stronger at higher energy. For example, if one requires $p_T^b > 20$ GeV, the acceptance in the 30 TeV setup for $|\eta| < 6$ is 69% and goes down to 8% for $|\eta| < 3$, while for $\sqrt{s} = 6$ TeV it goes from 70% to 32%, when moving the maximum rapidity from 6 to 3. In the lower part of table 3, we consider the additional cut $M_{HHH} < 1$ TeV. In this case the impact of the rapidity cut is milder, as can be expected by looking at figure 4. For instance, for $|y| < 3.0$ and $p_T^b > 20$ GeV the acceptance at $\sqrt{s} = 30$ TeV is about 8% without imposing any cut on the HHH invariant mass and becomes about 37% when the threshold region is considered.

We stress that, in table 3, we consider the purely geometric acceptances (i.e. we do not apply any branching ratio), which corresponds to work under the assumption that all the most relevant Higgs decay modes can be detected. Table 3 shows how the cuts on the transverse momentum and rapidity in the case of $6b$ -jet final state reduce the expected number of signal events, and point out the importance of having the largest possible rapidity coverage in the detector in order to measure the process under consideration. This point should be carefully taken into account in future detector studies.

\sqrt{s} [TeV]	3 TeV	6 TeV	10 TeV	14 TeV	30 TeV
$p_T^b > 0$ GeV					
$ y < 2.5$	0.4454 [0]	0.2123 [4]	0.1235 [10]	0.0880 [20]	0.0431 [80]
$ y < 3.0$	0.7055 [1]	0.4171 [8]	0.2626 [22]	0.1932 [45]	0.0990 [183]
$ y < 4.0$	0.9542 [1]	0.8548 [17]	0.7086 [60]	0.5904 [137]	0.3589 [664]
$ y < 5.0$	0.9957 [1]	0.9808 [20]	0.9522 [80]	0.9167 [213]	0.7521 [1392]
$ y < 6.0$	0.9999 [1]	0.9987 [20]	0.9950 [84]	0.9899 [230]	0.9585 [1774]
$p_T^b > 20$ GeV					
$ y < 2.5$	0.3431 [0]	0.1636 [3]	0.0956 [8]	0.0685 [16]	0.0338 [63]
$ y < 3.0$	0.5355 [1]	0.3178 [6]	0.2004 [17]	0.1479 [34]	0.0763 [141]
$ y < 4.0$	0.6925 [1]	0.6335 [13]	0.5292 [44]	0.4419 [103]	0.2695 [499]
$ y < 5.0$	0.7013 [1]	0.7003 [14]	0.6885 [58]	0.6681 [155]	0.5542 [1026]
$ y < 6.0$	0.7013 [1]	0.7018 [14]	0.7018 [59]	0.7019 [163]	0.6896 [1276]
$p_T^b > 0$ GeV, $M_{HHH} < 1$ TeV					
$ y < 2.5$	0.6712 [0]	0.5396 [1]	0.4563 [1]	0.4118 [2]	0.3309 [7]
$ y < 3.0$	0.8572 [1]	0.7479 [1]	0.6557 [2]	0.5984 [4]	0.4889 [14]
$ y < 4.0$	0.9821 [1]	0.9573 [3]	0.9182 [6]	0.8794 [11]	0.7697 [38]
$ y < 5.0$	0.9988 [1]	0.9955 [3]	0.9893 [7]	0.9816 [14]	0.9420 [56]
$ y < 6.0$	1.0000 [1]	0.9998 [3]	0.9992 [7]	0.9982 [15]	0.9924 [63]
$p_T^b > 20$ GeV, $M_{HHH} < 1$ TeV					
$ y < 2.5$	0.5144 [0]	0.4135 [1]	0.3494 [1]	0.3162 [2]	0.2537 [5]
$ y < 3.0$	0.6377 [1]	0.5590 [1]	0.4905 [2]	0.4490 [3]	0.3667 [11]
$ y < 4.0$	0.6979 [1]	0.6871 [2]	0.6630 [4]	0.6385 [8]	0.5610 [28]
$ y < 5.0$	0.6996 [1]	0.7006 [2]	0.6991 [5]	0.6971 [10]	0.6744 [41]
$ y < 6.0$	0.6996 [1]	0.7007 [2]	0.7008 [5]	0.7018 [11]	0.7011 [45]

Table 3: Ratio of the expected number of events with and without imposing acceptance cuts on the Higgs decay products for the energy setups in table 1. The Higgs bosons are produced on-shell and decayed to $b\bar{b}$ pairs but no branching ratio is applied. The numbers in square parenthesis are the expected number of events for the process $\mu^+\mu^- \rightarrow HHH\nu\bar{\nu}$ (the $H \rightarrow b\bar{b}$ branching ratio is not included) after imposing the cuts when assuming the integrated luminosities in table 1 for the c.m. energies under consideration. See main text for details.

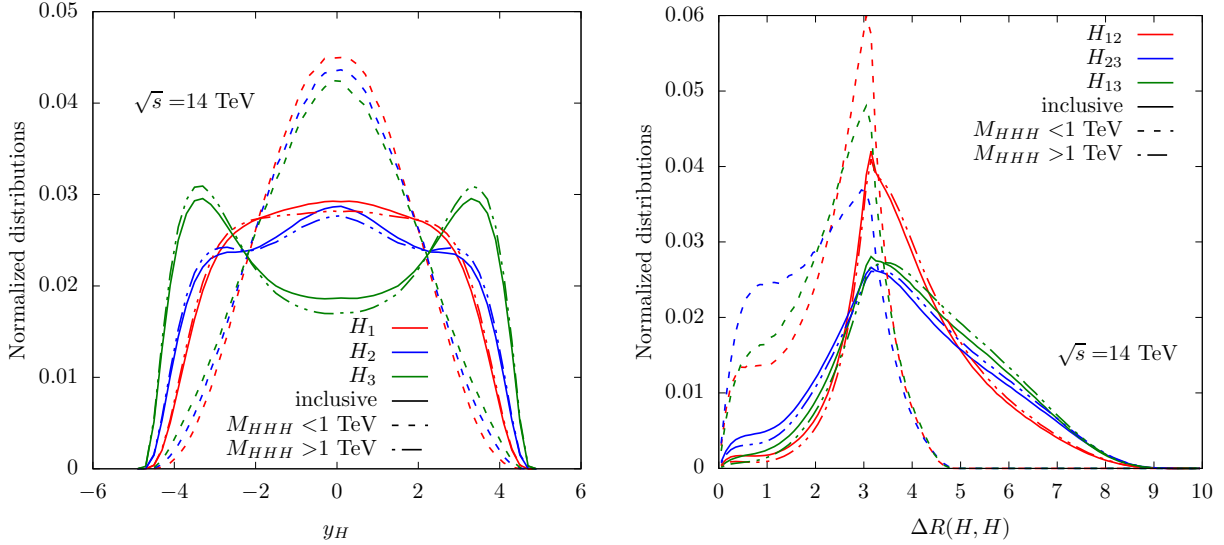


Figure 6: Higgs rapidity (left) and Higgs-pair ΔR (right) distributions in $\mu^+\mu^- \rightarrow HHH\nu\bar{\nu}$, in the SM, at $\sqrt{s} \simeq 14$ TeV, for $M_{\nu\nu} \gtrsim 150$ GeV. The index 1 refers to the highest- p_T Higgs, while the index 3 refers to the lowest- p_T Higgs. The solid lines stand for the inclusive distributions, the dashed (dotdashed) lines correspond to applying a further cut $M_{HHH} < (>) 1$ TeV.

3 Triple Higgs production with anomalous self-couplings

We can now pass to consider in detail how modifications of the trilinear and quartic couplings can modify cross sections and distributions. As already mentioned, the Feynman diagrams contributing to the process $\mu^+\mu^- \rightarrow HHH\nu\bar{\nu}$ can involve one quartic Higgs vertex or up to two Higgs trilinear vertices, see figure 1.

As a result, the most general expression for the cross section as a function of the deviations from the SM cubic and quartic Higgs couplings can be expressed in terms of a polynomial which is quartic in δ_3 and quadratic in δ_4 :

$$\sigma = c_1 + c_2\delta_3 + c_3\delta_4 + c_4\delta_3\delta_4 + c_5\delta_3^2 + c_6\delta_4^2 + c_7\delta_3^3 + c_8\delta_3^2\delta_4 + c_9\delta_3^4, \quad (9)$$

where the coefficients c_i can be obtained once for all from a MC simulation and they are collected in table 4, for the total cross sections with and without an upper cut on the HHH invariant mass of 1 TeV. This parametrization is useful for at least two reasons. The first is that it can be used to extract sensitivities to different scenarios without the need to rerun MC simulations for each benchmark point. The second advantage is that it is possible to directly gauge the sensitivity to new physics effects by comparing the value of the SM coefficient (c_1), with the linear terms c_2, c_3 , which are dominant for $\delta_{3,4} \ll 1$, and the quadratic (mixed or diagonal) terms ($c_{4,5,6}$), the cubic ($c_{7,8}$) and finally the quartic terms (c_9). First, the SM coefficient, as we had already seen in figure 2, grows faster than linearly, yet tends to flatten at high energy. As also seen before, the increase of the cross section is clearly provided by configurations which are far from threshold, and where at least one Higgs boson is soft and can be very forward. In fact, once an upper cut on the HHH invariant mass of 1 TeV is set, the increase on the cross sections is less than linear and very mild. Second, at the linear level and for total cross sections, the

$\sigma = c_1 + c_2\delta_3 + c_3\delta_4 + c_4\delta_3\delta_4 + c_5\delta_3^2 + c_6\delta_4^2 + c_7\delta_3^3 + c_8\delta_3^2\delta_4 + c_9\delta_3^4$					
\sqrt{s} (TeV)	3	6	10	14	30
c_i (ab)					
c_1	0.3127	1.6477	4.1820	7.0200	18.5124
c_2	-0.1533	-1.7261	-4.4566	-7.1000	-15.9445
c_3	-0.0753	-0.1159	-0.1166	-0.1147	-0.1117
c_4	-2.0566	-6.3052	-11.4981	-15.9807	-29.2794
c_5	4.7950	14.9060	27.1081	37.4658	67.7539
c_6	0.2772	0.8637	1.5992	2.2455	4.2038
c_7	-1.8353	-4.3210	-6.6091	-8.3962	-13.0964
c_8	0.5032	1.1861	1.8173	2.2967	3.5217
c_9	0.2943	0.5954	0.8946	1.1611	1.9349
$\bar{c}_i \equiv c_i(M_{HHH} < 1 \text{ TeV})$ (ab)					
\bar{c}_1	0.1165	0.2567	0.3743	0.4541	0.6404
\bar{c}_2	0.1667	0.3003	0.4046	0.3545	0.6972
\bar{c}_3	-0.0768	-0.1510	-0.2105	-0.2285	-0.3519
\bar{c}_4	-1.3604	-2.8996	-4.1522	-5.0582	-6.9538
\bar{c}_5	3.1017	6.6033	9.4721	11.4547	15.9505
\bar{c}_6	0.1842	0.3954	0.5679	0.6931	0.9543
\bar{c}_7	-1.5210	-3.0591	-4.3186	-4.8598	-7.3196
\bar{c}_8	0.4222	0.8550	1.2103	1.3906	2.0398
\bar{c}_9	0.2691	0.5482	0.7720	0.9702	1.2482

Table 4: Coefficients c_i , ruling the $\mu^+\mu^- \rightarrow HHH\nu_\mu\bar{\nu}_\mu$ cross-section dependence on the Higgs anomalous self-couplings δ_3 and δ_4 (as defined in the first row of the table), at different c.m. energies. The coefficients \bar{c}_i , entering the residual cross sections after applying a 1-TeV upper cut on the HHH invariant mass, are also detailed.

sensitivity to δ_4 is smaller than the one to δ_3 by a factor ranging between 2 to 100. On the other hand, if one focuses on events at threshold, there is a rather uniform difference of only a factor of two, the sign being opposite. This generically implies that positively correlated changes of the δ_4 and δ_3 , will be more difficult to constrain than variations in opposite directions. For example, in the SMEFT case where $\delta_4 = 6\delta_3$, there will be a cancellation, yet with the δ_4 contribution being dominating. More in general, the difference between the sensitivity at the inclusive level and at threshold, entails the possibility for flat directions in the parameter space to be lifted. Third, in presence of larger deviations, the higher-order terms in the polynomial could become the dominant effects. In this case, one notices that c_6 , corresponding to the δ_4^2 term, is always smaller than c_4 , the coefficient of the $\delta_3\delta_4$ term. This means that a joint departure of the trilinear and quartic term will be in general easier to detect, than that of the quartic alone.

Finally, we investigate the discriminating power of differential distributions, focusing our

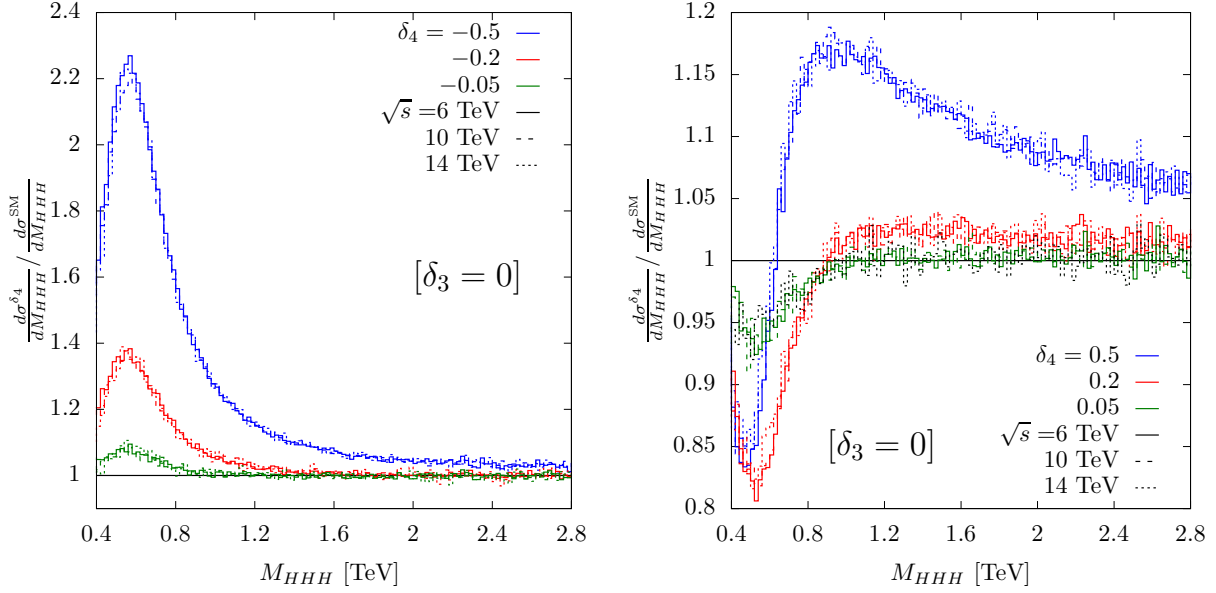


Figure 7: Dependence of the M_{HHH} distributions on a variation of the quartic Higgs coupling, for three energy setups, assuming $\delta_3 = 0$ (i.e., a SM trilinear self-coupling).

attention on the HHH invariant mass. In figure 7 we plot the ratio between the M_{HHH} distribution in a scenario where $\delta_3 = 0$, for $\delta_4 = -0.5, -0.2, -0.05$ (left plot) and for $\delta_4 = 0.5, 0.2, 0.05$ (right plot) for different c.m. energies. The first observation is the size as well as the dependence of the corrections on the M_{HHH} are very different between positive and negative values of δ_4 . The main reason can be traced back to the fact that even at the total integrated level the linear coefficient c_3 is negative while the quadratic coefficient c_6 is positive. For negative values of δ_4 the contributions sum and the final result is always larger than the SM, the larger effects being at threshold. For positive values of δ_4 , cancellations take place between the differential version of c_3 and c_6 , leading to a final non trivial pattern shown on the right plot: corrections start negative very close to threshold, and then become positive above about 600-800 GeV. In figure 8 we show the results of an analogous study, assuming $\delta_3 = -0.5, -0.2, -0.05$ (left plot) and $\delta_3 = 0.5, 0.2, 0.05$ with $\delta_4 = 6\delta_3$, i.e., in the SMEFT scenario. Also in this case the shape changes are larger at threshold and deviations with respect to SM predictions can be quite significant.

4 Sensitivity to the Higgs self-coupling deviations

We are now ready to perform the first exploration of the sensitivity of a future muon collider to deviations of the Higgs self-couplings.

For the sake of simplicity, we restrict the presentation to two possibly relevant scenarios:

- A) $\delta_3 = 0, \delta_4 \neq 0$, i.e., deviations only in the quartic Higgs coupling;
- B) $\delta_4 = 6\delta_3$, i.e., the pattern of deviations as expected from the SMEFT at dim=6.

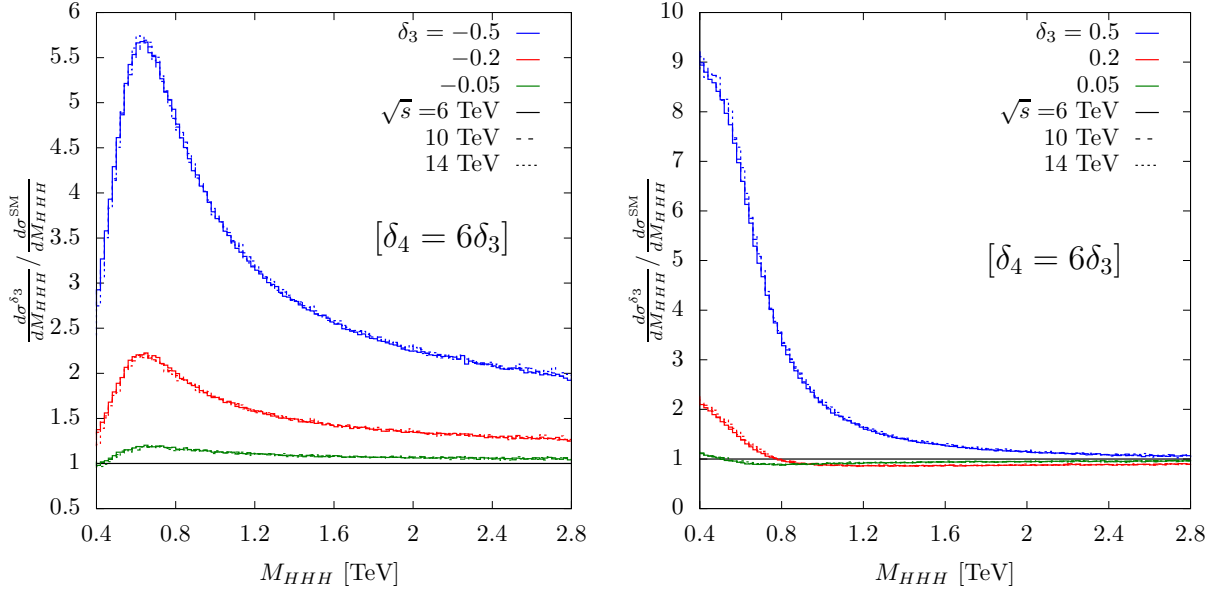


Figure 8: Dependence of the M_{HHH} distributions on a variation of the trilinear Higgs coupling, for three energy setups, assuming $\delta_4 = 6\delta_3$.

Scenario A assumes that no deviations on the trilinear coupling have been detected (and/or exist) and explores the possibility that new physics effects appear for the first time in the quartic self-coupling. Scenario B, on the other hand, assumes the SMEFT scaling between the two couplings. This scenario would fit the case where a deviation in the trilinear coupling is observed in other observables, such as in HH production. In this situation, an interesting question would be whether the deviation in δ_4 would follow the linear SMEFT pattern or not.

To provide a first estimation of the sensitivity, we focus on the signal process $\mu^+\mu^- \rightarrow HHH\nu\bar{\nu}$ and disregard possible backgrounds. In so doing, we are clearly setting an optimal target for more detailed future phenomenological and experimental investigations. We define the sensitivity to the non-SM Higgs couplings as:

$$\frac{|N - N_{\text{SM}}|}{\sqrt{N_{\text{SM}}}}, \quad (10)$$

where N_{SM} is the number of events assuming $\delta_3 = \delta_4 = 0$, while N is the number of events obtained for the values of δ_3 and δ_4 under consideration.

In figure 9 we show the dependence on δ_4 and δ_3 of the total cross section in two different bins, inclusive and for $M_{HHH} < 1$ TeV, and for the A (left) and B (right) scenarios (under the SM hypothesis), respectively. In both scenarios, one finds that the dependence on the anomalous couplings is weaker at high energy in the inclusive setup, while at threshold it is basically the same for all the c.m. energies under consideration. This is a consequence of the fact that the highest sensitivity is at threshold, while the region $M_{HHH} > 1$ TeV is much less sensitive to δ_3 and δ_4 and gives a contribution to the total cross section that increases with \sqrt{s} . This means that, as far as no further cuts are imposed on the Higgs decay products, increasing the energy brings an advantage mainly in the statistics. The results corresponding to independent variations of δ_3 and δ_4 are shown in figures 10, 11 and 12, where the red shaded

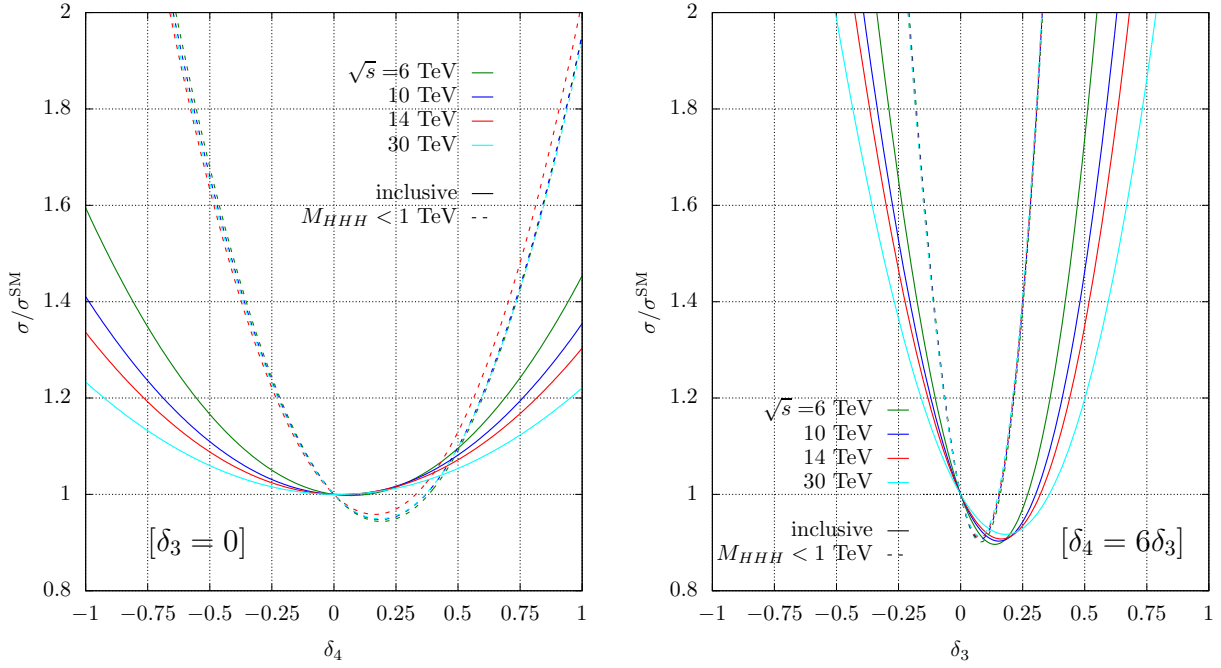


Figure 9: Dependence of the $\mu^+\mu^- \rightarrow HHH\nu\bar{\nu}$ cross section on the anomalous Higgs self-couplings in two different scenarios: A ($\delta_3 = 0$) on the left and B ($\delta_4 = 6\delta_3$) on the right. In the latter case the ratio of the cross sections is expressed in terms of δ_3 .

\sqrt{s} (TeV)	Lumi (ab^{-1})	Constraints on δ_4 (with $\delta_3 = 0$)		
		x-sec only 1 σ	x-sec only 2 σ	threshold + $M_{HHH} > 1$ TeV 1 σ
6	12	$[-0.60, 0.75]$	$[-0.90, 1.00]$	$[-0.55, 0.85]$
10	20	$[-0.50, 0.55]$	$[-0.70, 0.80]$	$[-0.45, 0.70]$
14	33	$[-0.45, 0.50]$	$[-0.60, 0.65]$	$[-0.35, 0.55]$
30	100	$[-0.30, 0.35]$	$[-0.45, 0.45]$	$[-0.20, 0.40]$
3	100	$[-0.35, 0.60]$	$[-0.50, 0.80]$	$[-0.45, 0.65]$

Table 5: Summary of the constraints on the quartic deviations δ_4 , assuming $\delta_3 = 0$, for various muon collider energy/luminosity options, as obtained from the total expected cross sections (1σ and 2σ CL). The third column shows the bounds obtained from the combination of the constraints corresponding to the setups $M_{HHH} < 1$ TeV and $M_{HHH} > 1$ TeV.

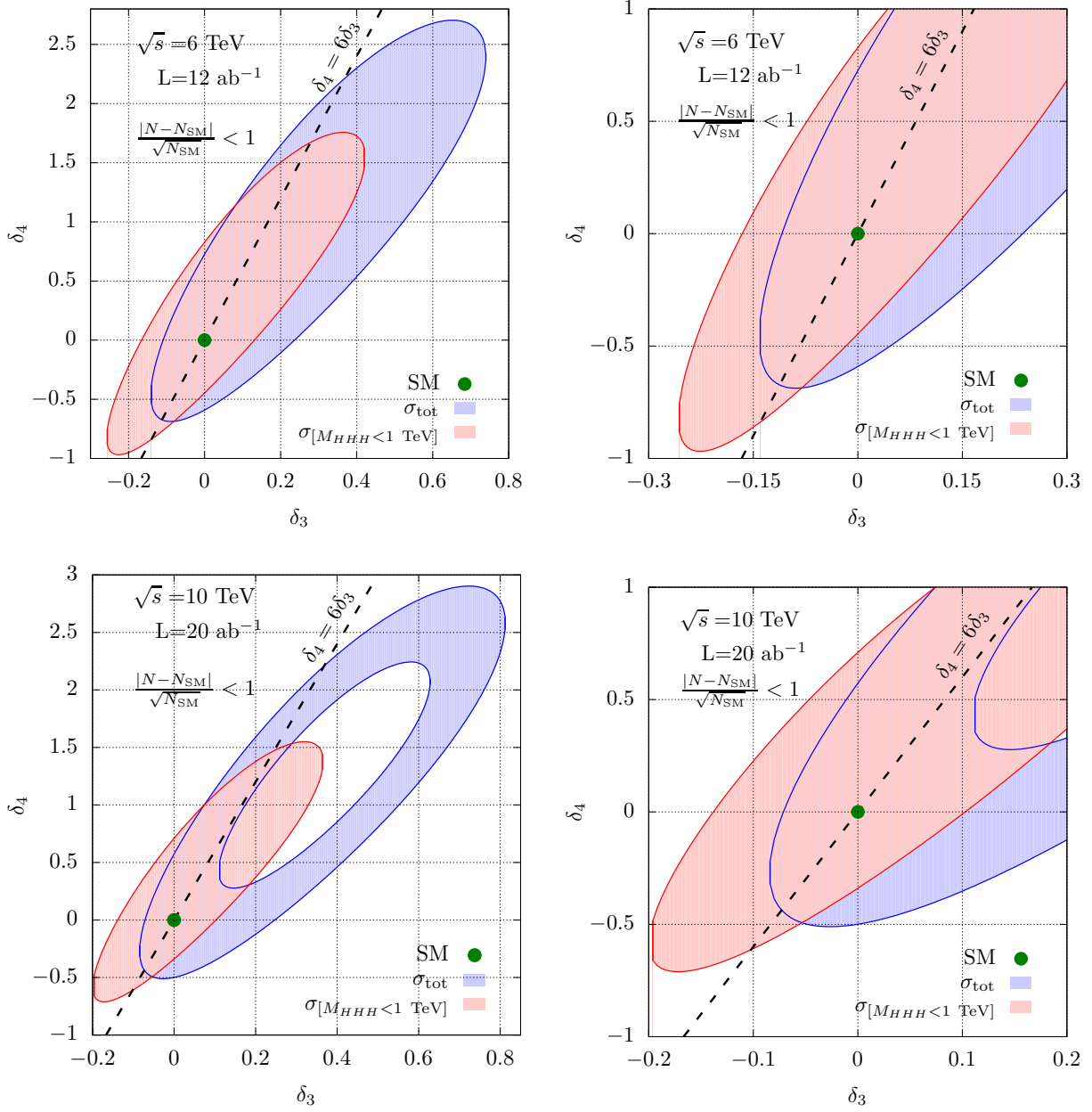


Figure 10: Left: 1- σ exclusion plots for the anomalous Higgs self-couplings in terms of the standard deviations $|N - N_{\text{SM}}|/\sqrt{N_{\text{SM}}}$ from the SM (green dot), where the event numbers N refer either to $\sigma(\mu^+\mu^- \rightarrow HHH\nu\bar{\nu})$, for $M_{\bar{\nu}\nu} \gtrsim 150\text{GeV}$ (blue area), or to the same cross section with an upper cut of 1 TeV on the HHH invariant mass (red area). Right: same plots zoomed around the SM configuration.

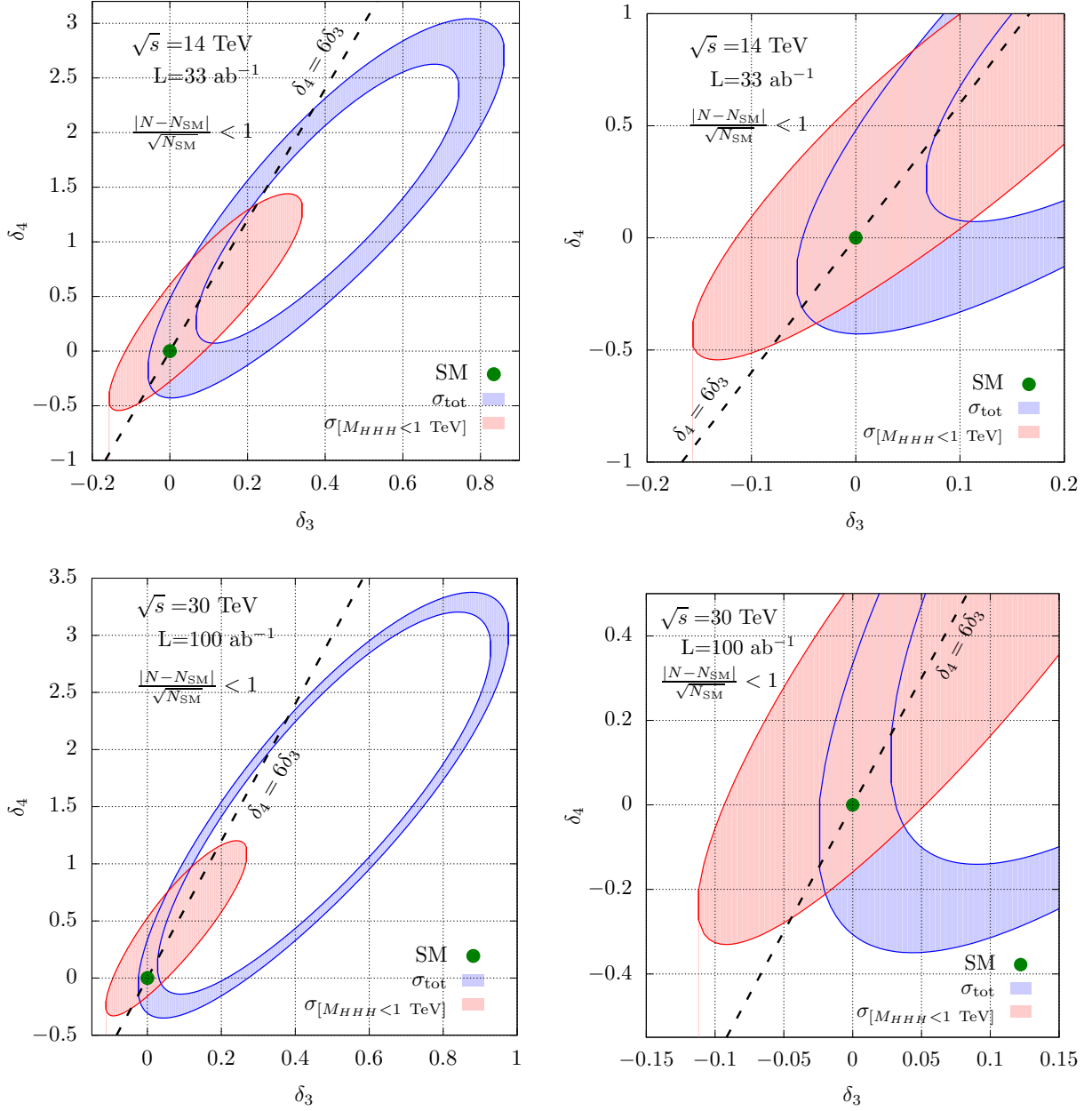


Figure 11: Left: 1- σ exclusion plots for the anomalous Higgs self-couplings in terms of the standard deviations $|N - N_{\text{SM}}|/\sqrt{N_{\text{SM}}}$ from the SM (green dot), where the event numbers N refer either to $\sigma(\mu^+\mu^- \rightarrow HHH\nu\bar{\nu})$, for $M_{\nu\bar{\nu}} \gtrsim 150\text{GeV}$ (blue area), or to the same cross section with an upper cut of 1 TeV on the HHH invariant mass (red area). Right: same plots zoomed around the SM configuration.

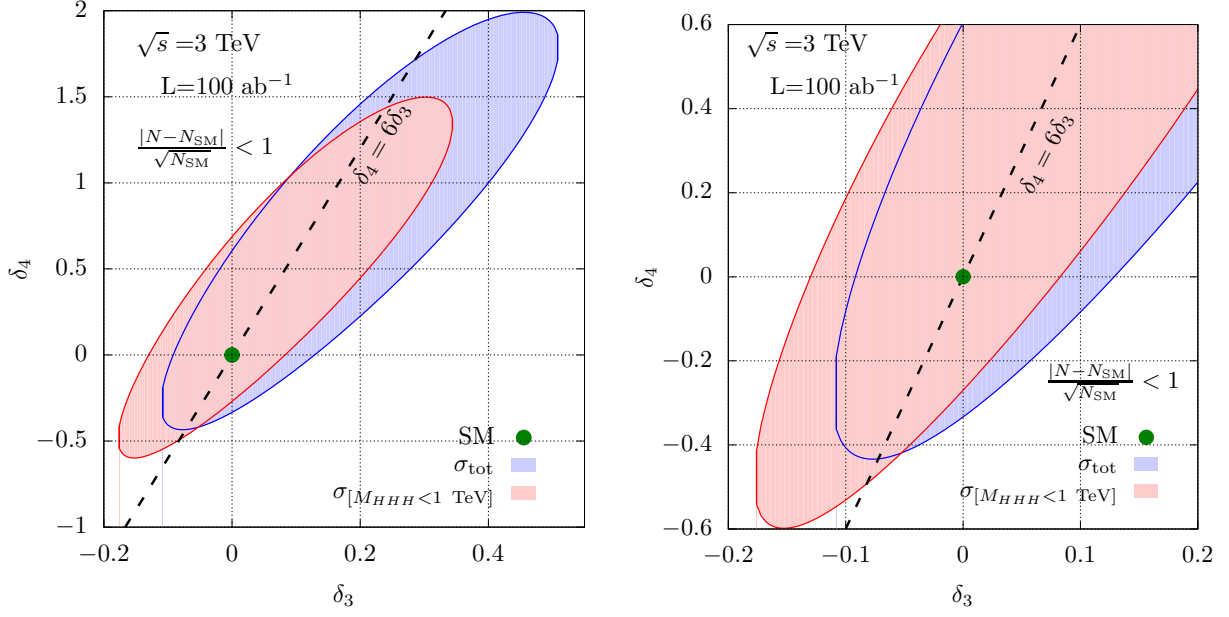


Figure 12: Left: $1\text{-}\sigma$ exclusion plot for the anomalous Higgs self-couplings in terms of the standard deviations $|N - N_{\text{SM}}|/\sqrt{N_{\text{SM}}}$ from the SM (green dot), where the event numbers N refer either to $\sigma(\mu^+\mu^- \rightarrow HHH\nu\bar{\nu})$, for $M_{\nu\bar{\nu}} \gtrsim 150\text{GeV}$ (blue area), or to the same cross section with an upper cut of 1 TeV on the HHH invariant mass (red area). Right: same plot zoomed around the SM configuration. The integrated luminosity assumed is about 20 times larger than the reference luminosity in table 1.

\sqrt{s} (TeV)	Lumi (ab^{-1})	Constraints on δ_4 (with $\delta_3 = 0$)		
		x-sec only, acceptance cuts		
		1σ	2σ	3σ
6	12	$[-0.50, 0.70]$	$[-0.74, 0.95]$	$[-0.93, 1.15]$
10	20	$[-0.37, 0.54]$	$[-0.55, 0.72]$	$[-0.69, 0.85]$
14	33	$[-0.28, 0.43]$	$[-0.42, 0.58]$	$[-0.52, 0.68]$
30	100	$[-0.15, 0.30]$	$[-0.24, 0.38]$	$[-0.30, 0.45]$
3	100	$[-0.34, 0.64]$	$[-0.53, 0.82]$	$[-0.67, 0.97]$

Table 6: Constraints on δ_4 ($\delta_3 = 0$) for the c.m. energies and the instantaneous luminosities in table 1 once the geometric acceptance cuts $p_T > 20$ GeV and $|\eta| < 3$ are applied to the Higgs decay products. The bounds are obtained from the total expected cross sections for the process $\mu^+\mu^- \rightarrow HHH\nu\bar{\nu}$. The Higgs bosons are produced on-shell and decayed to $b\bar{b}$ pairs but no branching ratio is applied.

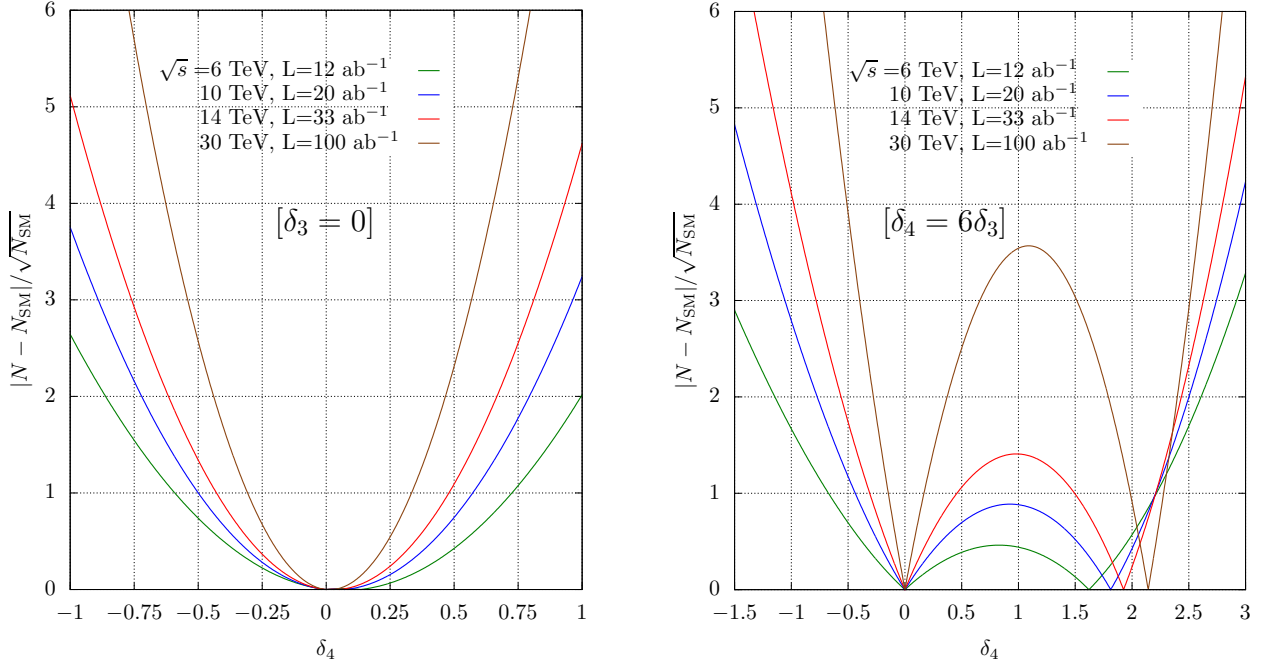


Figure 13: Sensitivity to the quartic Higgs self-coupling in terms of standard deviations $|N - N_{\text{SM}}|/\sqrt{N_{\text{SM}}}$ with respect to the SM configuration, where the event numbers N refer to $\sigma(\mu^+\mu^- \rightarrow HHH\nu\bar{\nu})$, for $M_{\nu\nu} \gtrsim 150\text{GeV}$, for $\delta_3 = 0$ (left), and $\delta_4 = 6\delta_3$ (right). Results are obtained considering deviations from the inclusive cross sections only.

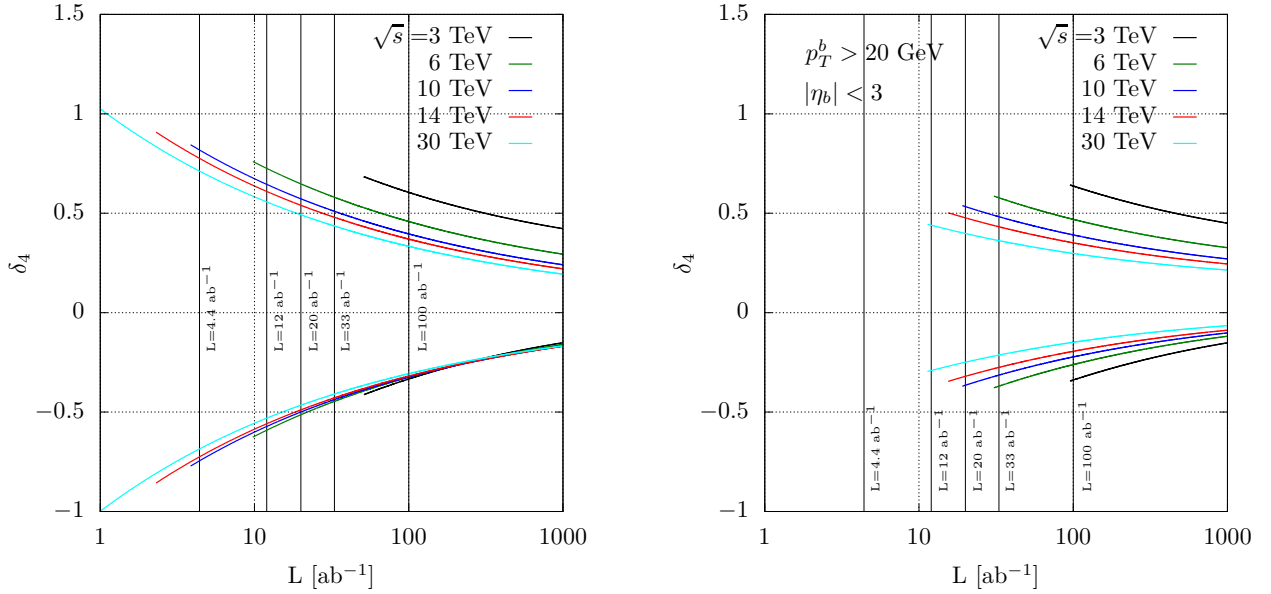


Figure 14: One-sigma constraints on δ_4 assuming $\delta_3 = 0$, for the c.m. energies in table 1, as a function of the integrated luminosity. The curves are obtained by requiring at least twenty signal events. The left plot corresponds to the inclusive setup, while in the right plot the Higgs decay products must have $p_T > 20\text{ GeV}$ and $|\eta| < 3$.

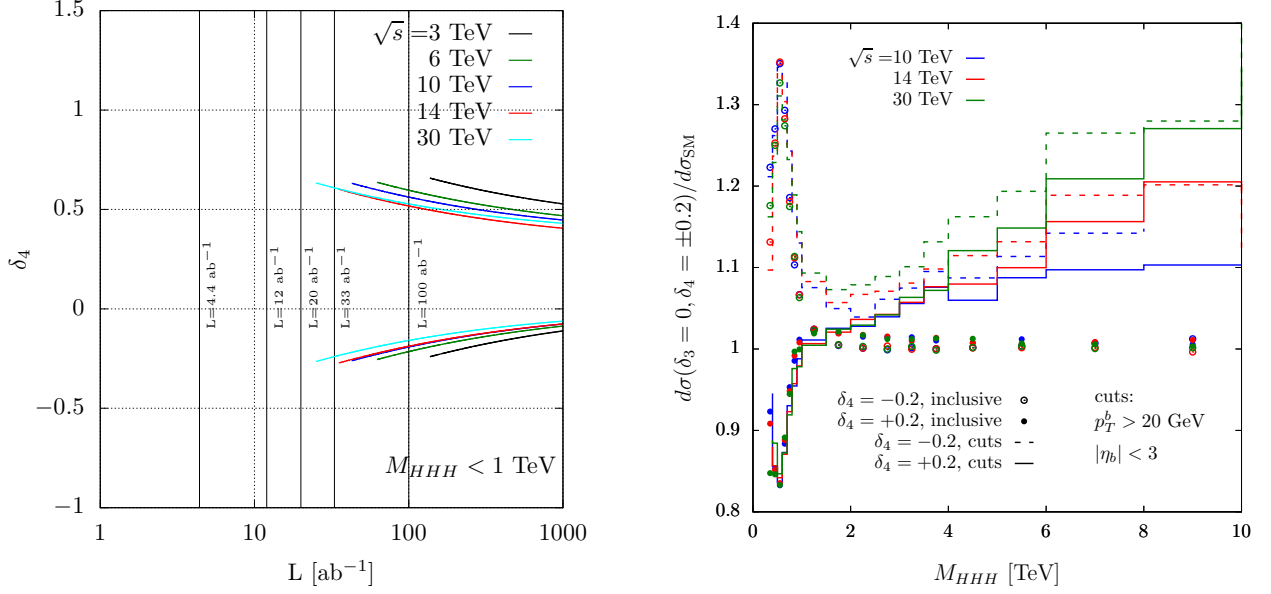


Figure 15: Left plot: one-sigma constraints on δ_4 in the threshold region ($M_{HHH} < 1$ TeV) assuming $\delta_3 = 0$, for the c.m. energies in table 1, as a function of the integrated luminosity. The curves are obtained by requiring at least twenty signal events. Right plot: ratios of the invariant mass distributions of the three Higgs bosons for $\delta_4 = \pm 0.2$ ($\delta_3 = 0$) and in the SM. The dots correspond to the inclusive setup, while the solid/dashed curves are obtained by imposing the geometric acceptance cuts on the Higgs decay products.

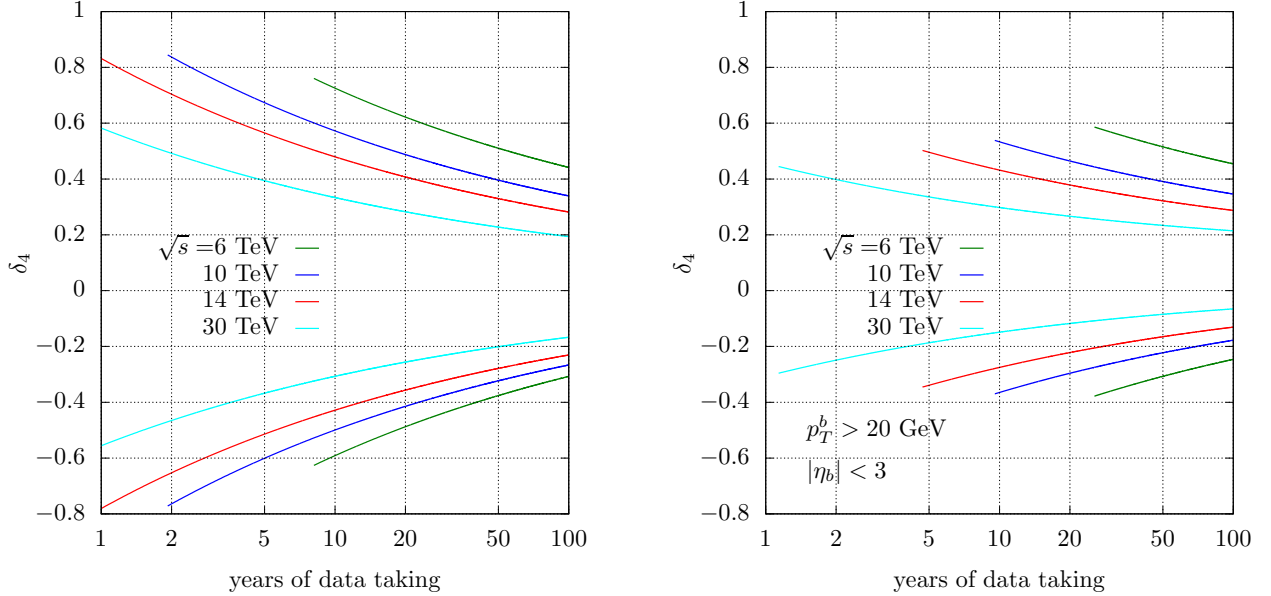


Figure 16: One-sigma constraints on δ_4 assuming $\delta_3 = 0$ for the c.m. energies and the instantaneous luminosities in table 1 as a function of the number of years of data taking. The curves are obtained by requiring at least twenty signal events. The left plot corresponds to the inclusive setup, while in the right plot the Higgs decay products must have $p_T > 20$ GeV and $|\eta| < 3$. The curves corresponding to the 3 TeV setup fall outside the time interval under consideration.

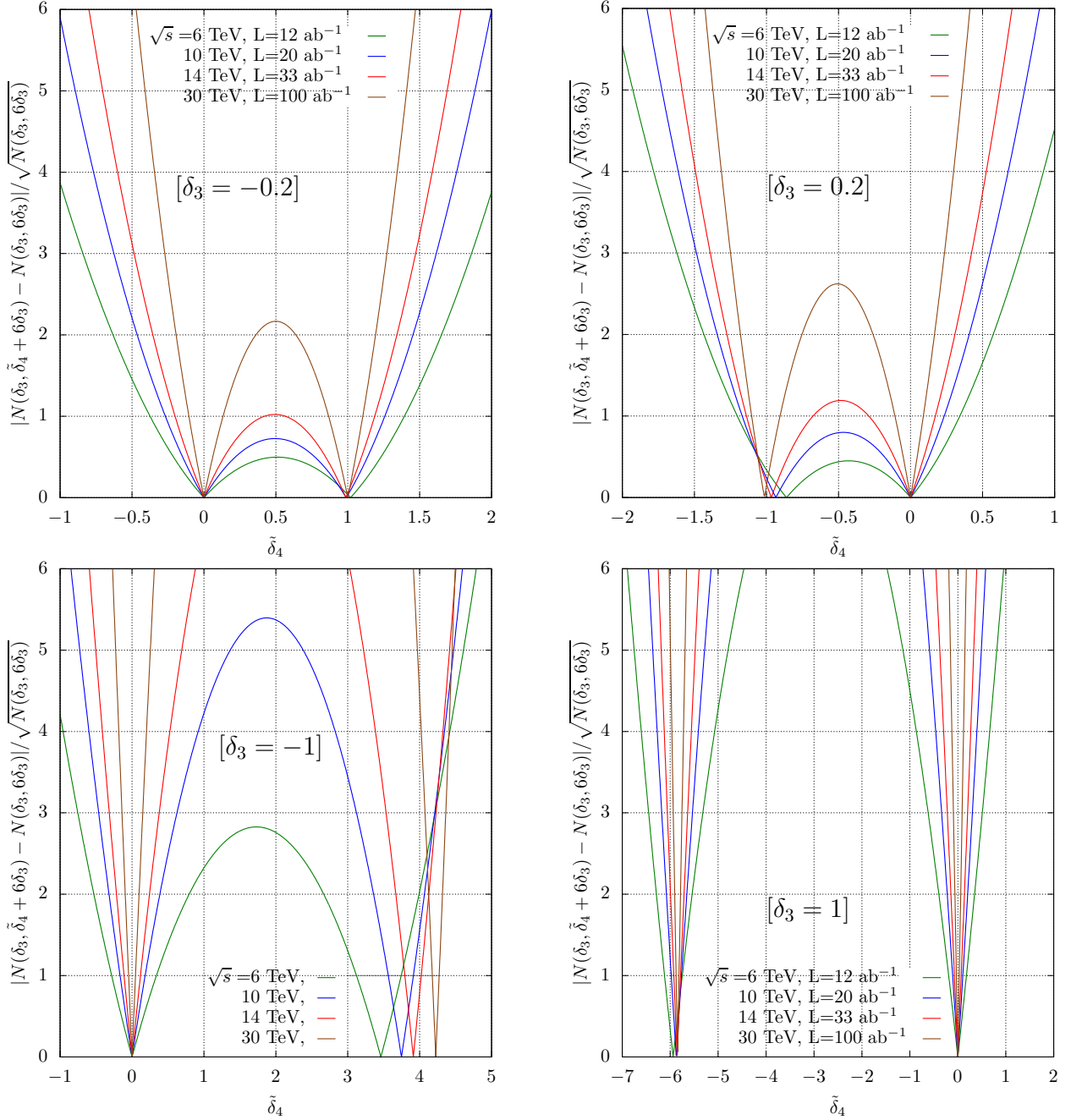


Figure 17: Sensitivity to $\tilde{\delta}_4 = \delta_4 - 6\delta_3$ in terms of standard deviations $|N(\delta_3, \tilde{\delta}_4 + 6\delta_3) - N(\delta_3, 6\delta_3)| / \sqrt{N(\delta_3, 6\delta_3)}$ with respect to the SMEFT configuration, where the event numbers N refer to $\sigma(\mu^+\mu^- \rightarrow HHH\nu\bar{\nu})$, for $M_{\nu\nu} \gtrsim 150\text{GeV}$. We assume $\delta_3 = -0.2$ (left), and $\delta_3 = 0.2$ (right) in the upper plots, and $\delta_3 = -1$ (left), and $\delta_3 = 1$ (right) in the lower plots. Results are obtained considering deviations from the inclusive cross sections.

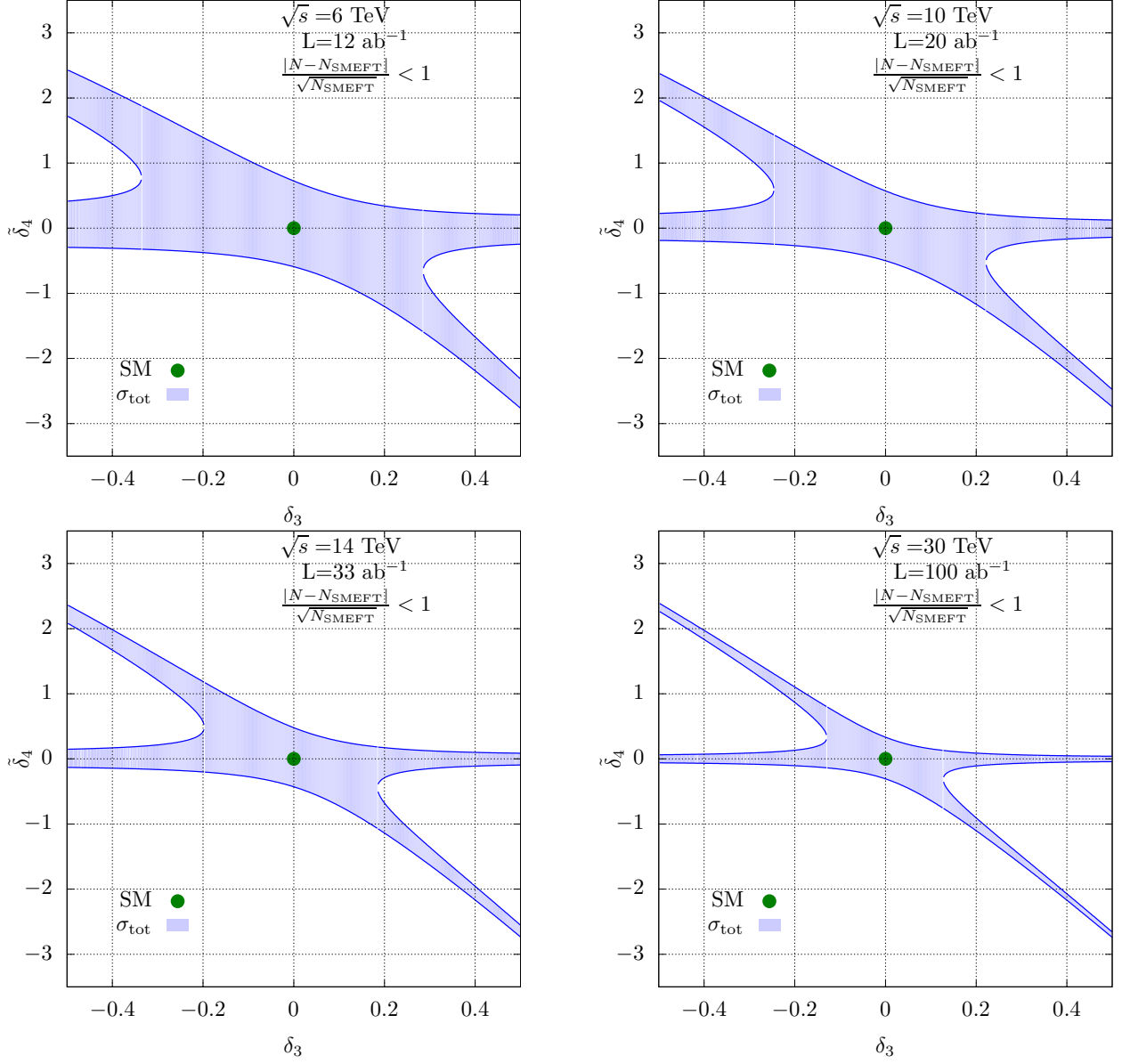


Figure 18: One-sigma exclusion plots in the $(\delta_3, \tilde{\delta}_4)$ plane in terms of standard deviations $|N(\delta_3, \tilde{\delta}_4 + 6\delta_3) - N(\delta_3, 6\delta_3)|/\sqrt{N(\delta_3, 6\delta_3)}$ with respect to the SMEFT configuration ($\tilde{\delta}_4 = \delta_4 - 6\delta_3$), for the c.m. energy of 6 (top left), 10 (top right), 14 (bottom left), and 30 TeV (bottom right). The generation cut $M_{\tilde{\nu}\nu} \gtrsim 150\text{GeV}$ is applied, but no cut is imposed on the Higgs bosons or their decay products.

areas correspond to the constraints obtained from threshold region, while the blue shaded areas correspond to the full sample. The plots on the right are blowups of the region close to the SM point (0,0). First, we note that as the energy increases, the blue areas tend to the shape of a ring in the plot range, showing the relevance of the quadratic terms and the fact that bounds are obtained from upper as well as lower limit in the number of events with respect to the SM expectations. As expected from the arguments given above, the constraints improve as the energy/luminosity increase mostly for the blue areas. In addition, the linear flat direction in the case of same sign variations of δ_3 and δ_4 are resolved by using two different regions and the higher terms in the c_i expansion. Figure 12 indicates that low energy runs, around 3 TeV, yet with a luminosity of 100 ab^{-1} could provide a determination in the range $-0.3 < \delta_4 < 0.6$ (with $\delta_3 = 0$).

Figure 13 presents the sensitivity in terms of number of standard deviations for $\sqrt{s} = 6, 10, 14$, and 30 TeV, assuming the integrated luminosities in table 1. In the case $\delta_3 = 0$ (left plot), it shows that a three-sigma constraint on δ_4 falls in the interval $[-1,1]$ for all the setups, with the only exception of $\sqrt{s} = 6$ TeV, where the δ_4 interval is slightly larger.

The constraints that can be obtained from the various energy/luminosity scenarios by using only information on the total cross section at 1σ and 2σ , and by combining events in the regions $M_{HHH} < 1 \text{ TeV}$ and $M_{HHH} > 1 \text{ TeV}$ (1σ), are summarized in table 5.

Figure 14 (left plot) shows the one-sigma exclusion limits on δ_4 (assuming $\delta_3 = 0$) for $\sqrt{s} = 3, 6, 10, 14$, and 30 TeV, varying the assumptions on the integrated luminosity. The curves are obtained requiring at least twenty signal events. As expected, the sensitivity to δ_4 improves when increasing the luminosity, rather moderately. Figure 14 (right plot) presents the same limits on δ_4 , but after imposing a minimum transverse momentum of 20 GeV and a maximum rapidity of 3 to the Higgs decay products. The message from this plot is twofold. On the one hand, the restriction in phase-space makes more difficult to reach the minimum number of events (20) required in the analysis (in particular, it needs to change the assumption on L for the 6 TeV setup from 12 ab^{-1} to about 30 ab^{-1}). On the other hand, interestingly, the plot also shows that the sensitivity to δ_4 improves when imposing a cut on the rapidity of the Higgs boson decay products. This is consequence of the fact that, while the SM production of three Higgs bosons tends to be forward, the effect of non-SM quartic Higgs couplings is mostly on central production, as one can naively expect from the behaviour of the amplitudes in presence of four-point interactions. Table 6 summarizes the constraints on δ_4 ($\delta_3 = 0$) that can be obtained by imposing the geometric acceptance cuts $p_T > 20 \text{ GeV}$ and $|\eta| < 3$ to the Higgs decay products for the c.m. energies and the instantaneous luminosities in table 1.

The one-sigma exclusion limits on δ_4 ($\delta_3 = 0$) in the threshold region are shown in figure 15 (left plot). By comparing figures 15 and 14, one can notice that, imposing only the threshold cut $M_{HHH} < 1 \text{ TeV}$, the required luminosity increases by a factor of about two and the sensitivity to positive values of δ_4 decreases, compared to the limits obtained under the geometric acceptance cuts on the Higgs decay products. These features can be explained by the fact that, while at low energies most of the central events that have the largest constraining power on δ_4 fall in the threshold region, for larger values of \sqrt{s} there is a non negligible fraction of central events with $M_{HHH} > 1 \text{ TeV}$. This can be read, for instance, from the right plot in figure 15, which shows the ratios of the M_{HHH} distributions computed for $\delta_4 = \pm 0.2$ ($\delta_3 = 0$) and in the SM for several c.m. energies both in the inclusive setup and after imposing a minimum transverse momentum

of 20 GeV and a maximum rapidity of 3 to the Higgs decay products: while in the inclusive setup the high invariant-mass tail is dominated by forward events and basically independent of δ_4 , when the acceptance cuts are imposed the ratios become positive for large invariant masses and increase with M_{HHH} . This happens for both positive and negative values of δ_4 . However, for $\delta_4 < 0$ most of the sensitivity corresponds to the positive peak at low invariant masses in figure 15. From the comparison of figures 14 and 15, we also notice that the sensitivity to δ_4 improves with the c.m. energy when the acceptance cuts are imposed, while the constraints on positive values of δ_4 are slightly more stringent at 14 TeV compared to the ones at 30 TeV if only the cut $M_{HHH} < 1$ TeV is applied. A similar behaviour can be found in figure 9, where the curve corresponding to $\sqrt{s} = 14$ TeV in the threshold region is above the one for $\sqrt{s} = 30$ TeV for $\delta_4 > 0$.

The plots in figure 16 are closely related to the ones in figure 14, and present the one-sigma constraints on δ_4 (when $\delta_3 = 0$) as a function of the number of years of data taking, both with and without cuts on the Higgs decay products, assuming the instantaneous luminosities in table 1. The curves corresponding to the 3 TeV setup fall outside the time interval under consideration.

In the present discussion, the underlying assumption for the setup $\delta_3 = 0$ is that no deviations are previously measured from the SM triple Higgs self-coupling. However, in case the study of HH production at the muon collider or at other machines will discover deviations from $\delta_3 = 0$, it would be interesting to search for possible deviations of δ_4 from its expected value in the SMEFT ($\tilde{\delta}_4 = \delta_4 - 6\delta_3$). As an example, the plots in figure 17 show the sensitivity to $\tilde{\delta}_4$ under the assumptions $\delta_3 = \mp 0.2$ and $\delta_3 = \mp 1$.

The one-sigma exclusion plots in the $(\delta_3, \tilde{\delta}_4)$ plane are presented in figure 18, for $\sqrt{s} = 6, 10, 14$, and 30 TeV assuming the integrated luminosities in table 1. The δ_3 range in the plots is motivated by the one-sigma limits on this parameter that can be reached at other future colliders, spanning from $\pm 50\%$ at HL-LHC and CEPC, to $\pm 10\%$ at CLIC and ILC at high energy, up to $\pm 5\%$ at FCC (we refer to [12, 10] for a summary of the exclusion limits on δ_3 at the proposed future machines). In the case of small deviations from the SM Higgs triple coupling, to each value of δ_3 corresponds an asymmetric interval in $\tilde{\delta}_4$ around $\tilde{\delta}_4 = 0$. Note that, for $\delta_3 = 0$, $\tilde{\delta}_4 = \delta_4$ and the bounds on $\tilde{\delta}_4$ are the same as the ones obtained in figures 10 and 11 for δ_4 . For larger values of δ_3 , the allowed region in $\tilde{\delta}_4$ becomes very narrow and splits into two disjoint intervals, one centered around $\tilde{\delta}_4 = 0$ and the other one in the negative (positive) $\tilde{\delta}_4$ region for $\delta_3 > 0$ ($\delta_3 < 0$).

5 Conclusions

Dreaming about a muon collider as a future option to study fundamental interactions of elementary particles at the energy frontier is becoming a widespread reality in the high-energy community. Technical obstacles that were previously thought as insurmountable are turned into formidable challenges worth to be investigated, wild expectations into ambitious goals at an increasing pace. In keep with the progress in understanding what could be really achieved at the accelerator and detector level in a not-too-far future, theoretical and phenomenological investigations are mandatory to fully establish the physics reach of a very high energy lepton

collider.

In this work, we have considered one of the most important and challenging task ahead of us in the on-going exploration and verification of the standard model, i.e., the characterization of the Higgs potential at low energy. Many studies exist on the perspectives to measure the trilinear Higgs self-coupling at future hadron and (up to 3 TeV) lepton colliders and there is a general expectation that a precision at a few percent level could be reached at some point. For this first exploration, we have therefore focused on the fourth derivative, the quartic self-coupling, whose determination is expected to be extremely difficult at all foreseen colliders.

We have considered in detail weak boson fusion production of three Higgs bosons, studying the sensitivity of total rates as well as of distributions on the Higgs boson self couplings. We have found good sensitivity in the threshold region, however, for the highest c.m. energy currently foreseen, the high energy tail provides most of the statistics and allows to improve the sensitivity to δ_4 by restricting the acceptance to the central region. We have then considered various possible scenarios attainable in different energy/luminosity configurations and determined the limits on the trilinear and quartic couplings in two motivated reference scenarios. Even though we adopted (theoretical as well as experimental) simplifying assumptions, we reckon to have identified the most important features of this process. In particular, we have verified that even in the case where the forward regions become difficult to access due to machine backgrounds, the sensitivity would not worsen as mostly coming from events central in the detector. This preliminary result supports the hope that the possible worsening of the sensitivity from a more realistic analysis including, for instance, backgrounds and systematic uncertainties, might be offset by many possible improvements both in analyses optimisation and in detector development.

Our results give a first indication that a leptonic collider at several TeV's of c.m. energy and with integrated luminosities of the order of a few tens of attobarns, could provide enough events to allow a determination of the (SM) Higgs quartic self-coupling with an accuracy in the tens of percent. For example, assuming $\lambda_3 = \lambda_{SM}$, and a (14 TeV/33 ab⁻¹) scenario, one could constrain λ_4 with a 50% uncertainty at 1σ , i.e., significantly better than what is currently expected to be attainable at the FCC-hh with a similar luminosity.

To finally assess the reach of a multi-TeV muon collider many more (and more detailed) studies will be necessary. This first work on the determination of the quartic self-coupling of the Higgs suggests that such studies are certainly worth to be undertaken.

Acknowledgments

We thank Nadia Pastrone, Jean-Pierre Delahaye, Thorsten Ohl, Donatella Lucchesi, and Andrea Wulzer for useful discussions. This work has received funding from the European Union's Horizon 2020 research and innovation programme as part of the Marie Skłodowska-Curie Innovative Training Network MCnetITN3 (grant agreement no. 722104). The work of M. C. has been supported by the Investissements d'avenir, Labex ENIGMASS.

References

- [1] G. Aad et al. [ATLAS Collaboration], *Observation of a new particle in the search for the Standard Model Higgs boson with the ATLAS detector at the LHC*, Phys. Lett. B **716** (2012), 1-29 [arXiv:1207.7214 [hep-ex]].
- [2] S. Chatrchyan et al. [CMS Collaboration], *Observation of a New Boson at a Mass of 125 GeV with the CMS Experiment at the LHC*, Phys. Lett. B **716** (2012), 30-61 [arXiv:1207.7235 [hep-ex]].
- [3] A. M. Sirunyan et al. [CMS Collaboration], *Combined measurements of Higgs boson couplings in proton–proton collisions at $\sqrt{s} = 13$ TeV*, Eur. Phys. J. C **79** (2019) no.5, 421 [arXiv:1809.10733 [hep-ex]].
- [4] G. Aad et al. [ATLAS Collaboration], *Combined measurements of Higgs boson production and decay using up to 80 fb⁻¹ of proton–proton collision data at $\sqrt{s} = 13$ TeV collected with the ATLAS experiment*, Phys. Rev. D **101** (2020) no.1, 012002 [arXiv:1909.02845 [hep-ex]].
- [5] F. Englert and R. Brout, *Broken Symmetry and the Mass of Gauge Vector Mesons*, Phys. Rev. Lett. **13** (1964), 321-323.
- [6] P. W. Higgs, *Broken symmetries, massless particles and gauge fields*, Phys. Lett. **12** (1964), 132-133.
- [7] P. W. Higgs, *Broken Symmetries and the Masses of Gauge Bosons*, Phys. Rev. Lett. **13** (1964), 508-509.
- [8] G. Guralnik, C. Hagen and T. Kibble, *Global Conservation Laws and Massless Particles*, Phys. Rev. Lett. **13** (1964), 585-587.
- [9] M. Cepeda et al., *Report from Working Group 2*, CERN Yellow Rep. Monogr. **7** (2019), 221-584 [arXiv:1902.00134 [hep-ph]].
- [10] J. de Blas, M. Cepeda, J. D’Hondt, R. Ellis, C. Grojean, B. Heinemann, F. Maltoni, A. Nisati, E. Petit, R. Rattazzi and W. Verkerke, *Higgs Boson Studies at Future Particle Colliders*, JHEP **01** (2020), 139 [arXiv:1905.03764 [hep-ph]].
- [11] P. Agrawal, D. Saha, L. Xu, J. Yu and C. Yuan, *Determining the Shape of Higgs Potential at Future Colliders*, [arXiv:1907.02078 [hep-ph]].
- [12] B. Di Micco et al., *Higgs Boson Pair Production at Colliders: Status and Perspectives*, [arXiv:1910.00012 [hep-ph]].
- [13] A. Abada et al. [FCC Collaboration], *FCC Physics Opportunities*, Eur. Phys. J. C **79** (2019) no.6, 474.
- [14] A. Abada et al. [FCC Collaboration], *FCC-ee: The Lepton Collider*, Eur. Phys. J. ST **228** (2019) no.2, 261-623.

- [15] A. Abada et al. [FCC Collaboration], *FCC-hh: The Hadron Collider*, Eur. Phys. J. ST **228** (2019) no.4, 755-1107.
- [16] F. Maltoni, D. Pagani and X. Zhao, *Constraining the Higgs self-couplings at ee colliders*, JHEP **07** (2018), 087 [arXiv:1802.07616 [hep-ph]].
- [17] W. Bizoń, U. Haisch and L. Rottoli, *Constraints on the quartic Higgs self-coupling from double-Higgs production at future hadron colliders*, JHEP **10** (2019), 267 [arXiv:1810.04665 [hep-ph]].
- [18] S. Borowka, C. Duhr, F. Maltoni, D. Pagani, A. Shivaji and X. Zhao, *Probing the scalar potential via double Higgs boson production at hadron colliders*, JHEP **04** (2019), 016 [arXiv:1811.12366 [hep-ph]].
- [19] A. Papaefstathiou and K. Sakurai, *Triple Higgs boson production at a 100 TeV proton–proton collider*, JHEP **02** (2016), 006 [arXiv:1508.06524 [hep-ph]].
- [20] R. Contino et al., *Physics at a 100 TeV pp collider: Higgs and EW symmetry breaking studies*, CERN Yellow Rep. (2017) no.3, 255-440 [arXiv:1606.09408 [hep-ph]].
- [21] B. Fuks, J. H. Kim and S. J. Lee, *Scrutinizing the Higgs quartic coupling at a future 100 TeV proton–proton collider with taus and b-jets*, Phys. Lett. B **771** (2017), 354-358 [arXiv:1704.04298 [hep-ph]].
- [22] A. Papaefstathiou, G. Tetlalmatzi-Xolocotzi and M. Zaro, *Triple Higgs boson production to six b-jets at a 100 TeV proton collider*, Eur. Phys. J. C **79** (2019) no.11, 947 [arXiv:1909.09166 [hep-ph]].
- [23] R. K. Ellis et al., *Physics Briefing Book : Input for the European Strategy for Particle Physics Update 2020*, [arXiv:1910.11775 [hep-ex]].
- [24] J. P. Delahaye, M. Diemoz, K. Long, B. Mansoulié, N. Pastrone, L. Rivkin, D. Schulte, A. Skrinsky and A. Wulzer, *Muon Colliders*, [arXiv:1901.06150 [physics.acc-ph]].
- [25] V. Shiltsev and F. Zimmermann, *Modern and Future Colliders*, [arXiv:2003.09084 [physics.acc-ph]].
- [26] V. Shiltsev, *Future Muon Colliders, Higgs and Neutrino Factories*, doi:10.2172/1571797.
- [27] N. Bartosik et al., *Preliminary Report on the Study of Beam-Induced Background Effects at a Muon Collider*, [arXiv:1905.03725 [hep-ex]].
- [28] D. Lucchesi, *Challenges and perspectives for a muon collider*, talk at the 105th Plenary ECFA meeting - CERN, 14-15 Nov 2019, <https://indico.cern.ch/event/847002/>.
- [29] M. Palmer, *Status of systems R&D for high-intensity muon accelerators*, talk at the 105th Plenary ECFA meeting - CERN, 14-15 Nov 2019, <https://indico.cern.ch/event/847002/>.

- [30] D. Schulte, *Conceptual design and future plans*, talk at the 105th Plenary ECFA meeting - CERN, 14-15 Nov 2019, <https://indico.cern.ch/event/847002/>.
- [31] M. Antonelli, M. Boscolo, R. Di Nardo and P. Raimondi, *Novel proposal for a low emittance muon beam using positron beam on target*, Nucl. Instrum. Meth. A **807** (2016), 101-107 [arXiv:1509.04454 [physics.acc-ph]].
- [32] D. Alesini et al., *Positron driven muon source for a muon collider*, [arXiv:1905.05747 [physics.acc-ph]].
- [33] A. Conway, H. Wenzel, R. Lipton and E. Eichten, *Measuring the Higgs Self-Coupling Constant at a Multi-TeV Muon Collider*, [arXiv:1405.5910 [hep-ex]].
- [34] M. Moretti, T. Ohl and J. Reuter, *O'Mega: An Optimizing matrix element generator*, [arXiv:hep-ph/0102195 [hep-ph]].
- [35] W. Kilian, T. Ohl and J. Reuter, *WHIZARD: Simulating Multi-Particle Processes at LHC and ILC*, Eur. Phys. J. C **71** (2011), 1742 [arXiv:0708.4233 [hep-ph]].
- [36] J. Alwall et al., *The automated computation of tree-level and next-to-leading order differential cross sections, and their matching to parton shower simulations*, JHEP **07** (2014), 079 [arXiv:1405.0301 [hep-ph]].
- [37] G. W. Foster and N. V. Mokhov, *Backgrounds and detector performance at a 2×2 TeV $\mu^+\mu^-$ collider*, AIP Conf. Proc. **352** (1996), 178-190
- [38] C. Johnstone and N. Mokhov, *Optimization of a muon collider interaction region with respect to detector backgrounds and the heat load to the cryogenic systems*, eConf **C960625** (1996), ACC030 FERMILAB-CONF-96-366.
- [39] N. V. Mokhov and S. I. Striganov, *Detector Background at Muon Colliders*, Phys. Procedia **37** (2012) 2015 doi:10.1016/j.phpro.2012.03.761 [arXiv:1204.6721 [physics.ins-det]].
- [40] Y. I. Alexahin et al., *Muon collider interaction region design*, Phys. Rev. ST Accel. Beams **14** (2011), 061001 [arXiv:1204.5739 [physics.acc-ph]].
- [41] N. V. Mokhov, S. I. Striganov and I. S. Tropin, *Reducing Backgrounds in the Higgs Factory Muon Collider Detector*, doi:10.18429/JACoW-IPAC2014-TUPRO029 arXiv:1409.1939 [physics.ins-det].